

Published in final edited form as:

*Cell Stem Cell.* 2019 February 07; 24(2): 328–341.e9. doi:10.1016/j.stem.2018.11.014.

## Deterministic Somatic Cell Reprogramming Involves Continuous Transcriptional Changes Governed by Myc and Epigenetic-Driven Modules

Asaf Zviran<sup>#1,2</sup>, Nofar Mor<sup>#1</sup>, Yoach Rais<sup>#1</sup>, Hila Gingold<sup>1</sup>, Shani Peles<sup>1</sup>, Elad Chomsky<sup>1,3,4</sup>, Sergey Viukov<sup>1</sup>, Jason D. Buenrostro<sup>5,6</sup>, Roberta Scognamiglio<sup>7</sup>, Leehee Weinberger<sup>1</sup>, Yair S. Manor<sup>1</sup>, Vladislav Krupalnik<sup>1</sup>, Mirie Zerbib<sup>1</sup>, Hadas Hezroni<sup>3</sup>, Diego Adhemar Jaitin<sup>8</sup>, David Larastiaso<sup>8</sup>, Shlomit Gilad<sup>9</sup>, Sima Benjamin<sup>9</sup>, Ohad Gafni<sup>1</sup>, Awni Mousa<sup>1</sup>, Muneef Ayyash<sup>1</sup>, Daoud Sheban<sup>1</sup>, Jonathan Bayerl<sup>1</sup>, Alejandro Aguilera Castrejon<sup>1</sup>, Rada Massarwa<sup>1</sup>, Itay Maza<sup>1,10</sup>, Suhair Hanna<sup>1,11</sup>, Yonatan Stelzer<sup>13</sup>, Igor Ulitsky<sup>3</sup>, William J. Greenleaf<sup>13,14</sup>, Amos Tanay<sup>3,4</sup>, Andreas Trumpp<sup>7</sup>, Ido Amit<sup>7</sup>, Yitzhak Pilpel<sup>1</sup>, Noa Novershtern<sup>1,#</sup>, Jacob H. Hanna<sup>1,#,%</sup>

<sup>1</sup>Department of Molecular Genetics, Weizmann Institute of Science, Rehovot 761001, Israel

<sup>2</sup>New York Genome Center, New York, NY, USA

<sup>3</sup>Department of Biological Regulation, Weizmann Institute of Science, Rehovot, Israel

<sup>4</sup>Department of Computer Science, Weizmann Institute of Science, Rehovot, Israel

<sup>5</sup>Broad Institute of MIT and Harvard, Cambridge, MA, USA

<sup>6</sup>Harvard Society of Fellows, Harvard University, Cambridge, MA, USA

<sup>7</sup>Heidelberg Institute for Stem Cell Technology and Experimental Medicine, DKFZ German Cancer Research Center, Heidelberg, Germany

<sup>8</sup>Department of Immunology, Weizmann Institute of Science, Rehovot, Israel

<sup>9</sup>INCPM, Weizmann Institute of Science, Rehovot, Israel

<sup>10</sup>Department of Gastroenterology, Rambam Hospital, Haifa, Israel

<sup>11</sup>Department of Pediatrics, Rambam Hospital, Haifa, Israel

### Author Contribution

A.Z., N.M., Y.R., N. N. and J.H.H. conceived the idea for this project, conducted experiments and wrote the manuscript. M.Z., R.M. and Y.R. conducted micro-injections. S.B. and S.G. conducted and supervised high-throughput sequencing. A.M. and Y.S.M. assisted in RNA-seq analysis. I.U. and H.H. conducted lncRNA analysis. W.J.G. and J.B. assisted in analyzing ATAC-seq. E.C. and A.T. assisted in WGBS. H.G. and A.Z. performed tRNA analysis under the supervision of Y.P. I.A., D.A. and D.J. assisted in ChIP-seq experiments. N.N. supervised bioinformatics and analyzed ChIP-seq data. S.P., M.A., I.M., S.H., A.A., J.B., D.S. and V.K. assisted in tissue culture. Y.S. assisted in RGM reporter experiments. Y.R., L.W. and N.M. engineered cell lines under S.V. supervision. A.T. and R.S. provided Myc mutant lines. N.N. and J.H.H. supervised executions of experiments and adequate analysis of data.

Correspondence to: Yoach Rais; Noa Novershtern; Jacob H. Hanna.

<sup>#</sup>Correspondence: Jacob Hanna (jacob.hanna@weizmann.ac.il), Noa Novershtern (noa.novershtern@weizmann.ac.il), Yoach Rais (yoach.rais@weizmann.ac.il).

<sup>#</sup>Senior authors.

<sup>%</sup>Lead contact

### Declaration of interests

J.H.H. is an advisor to Biological Industries Ltd. J.H.H., N.N., and Y.R. filed related patents.

<sup>12</sup>Department of Molecular and Cell Biology, Weizmann Institute of Science, Rehovot, Israel

<sup>13</sup>Department of Genetics, Stanford University, Palo Alto, CA, USA

<sup>14</sup>Chan Zuckerberg Biohub, San Francisco, CA, USA

# These authors contributed equally to this work.

## Abstract

The epigenetic dynamics of iPSC reprogramming in correctly reprogrammed cells at high resolution and throughout the entire process, remain largely undefined. Here we characterize conversion of mouse fibroblasts into iPSCs using *Gatad2a*-*Mbd3*/NuRD depleted and highly efficient reprogramming systems. Unbiased high-resolution profiling of dynamic changes in levels of gene expression, chromatin engagement, DNA accessibility and DNA methylation were obtained. We identified two distinct and synergistic transcriptional modules that dominate successful reprogramming, which are associated with pluripotency and biosynthetic genes respectively. The pluripotency module is governed by dynamic alterations in epigenetic modifications to promoters and binding by Oct4, Sox2 and Klf4. Early DNA demethylation at these enhancers prospectively marks cells fated to reprogram. Myc activity drives expression of the essential biosynthetic module and is associated with changes in tRNA codon usage. Our functional validations highlight interweaved epigenetic- and Myc-governed essential reconfigurations that rapidly commission and propel deterministic reprogramming toward naïve pluripotency.

## Introduction

The ability to reprogram somatic cells into induced pluripotent stem cells (iPSCs) with Oct4, Sox2, Klf4 and Myc (abbreviated as OSKM) (Takahashi and Yamanaka, 2006) has provoked interest to define the molecular characteristics of this process. Previous epigenetic mapping studies on iPSC reprogramming were conducted on inefficient and a-synchronized systems undergoing protracted reprogramming (Hussein et al., 2014) or by sorting pre-iPSCs, most of which do not progress to become iPSCs. However, this low-efficiency and heterogeneity has limited genome-wide analysis of well-characterized, relatively homogeneous populations of cells that successfully complete this process.

Our group has demonstrated that optimized hypomorphic depletion of *Mbd3* or *Gatad2a*, representing core members of the *Gatad2a*-*Chd4*-*Mbd3*/NuRD repressor complex, results in deterministic up to 100% efficient and more synchronized reprogramming in mouse cells within 8 days (Rais et al., 2013, Mor et al., 2018). Such systems enable high-resolution temporal dissection of epigenetic dynamics underlying conducive naïve iPSC formation, while simultaneously reducing ‘noise’ from heterogeneous populations that fail to correctly complete the reprogramming course. With this opportunity to map epigenetics of reprogramming towards ground state naïve pluripotency in highly efficient and homogenous systems, without cell passaging or sorting for sub-populations, we provide comprehensive characterization during the entire 8-day course of fibroblast reprogramming.

## Results and Discussion

### Mapping deterministic reprogramming

We analyzed reprogramming of two independently generated *Mbd3<sup>f/-</sup>* and *Gatad2a<sup>-/-</sup>* secondary MEF clonal systems, carrying a doxycycline (DOX) inducible human OKSM transgene. Cells were harvested every 24 hours until day 8, in which they are fully reprogrammed, and processed for library preparation and sequencing. Two WT MEF secondary reprogramming systems (WT-1 and WT-2) were used as controls, where WT-2 is an isogenic genetically matched cell line to the *Gatad2a<sup>-/-</sup>* cells (Mor et al., 2018; Rais et al., 2013). The use of independent *Mbd3*- and *Gatad2a*-depleted highly efficient systems with different single copy OKSM transgene integration pattern, excludes cell line specific signatures (Fig. S1A). We sequenced 212 libraries from the NuRD depleted systems and 21 libraries from WT1/2 systems (Table S1). The libraries span transcriptome (RNA-seq, small RNA-seq), chromatin modifications (ChIP-seq for H3K27ac, H3K27me3, H3K4me1, H3K4me3, H3K36me3, H3K9me2, H3K9me3), DNA methylation, chromatin accessibility (ATAC-seq) and factor binding (Oct4, Sox2, Klf4, c-Myc and RNA-PolII ChIP-seq). Overall, we aligned 12.12 billion reads (Table S1). RNA-seq samples were reproducible with average correlation of  $R=0.93$  between consecutive samples (Fig. 1B-C). TF and chromatin modification ChIP-seq samples showed high overlap between consecutive samples (Jaccard index  $>0.3$ , Fig. 1D-E). iPSC and ESC samples showed high consistency with previous measurements (Fisher exact test  $p<10^{-4}$ , Fig. 1F).

### Deterministic reprogramming is accompanied by continuous transcriptional changes

Gene expression profiles in *Mbd3<sup>f/-</sup>* and *Gatad2a<sup>-/-</sup>* systems were highly similar (average  $R=0.88$  in Fig. 1C,G; Tables S2-S3). To further evaluate the kinetics of the two systems, we compared them to two WT secondary reprogramming systems (WT-2 series is isogenic to *Gatad2a<sup>-/-</sup>* series), and to some of the previously published datasets which mapped iPSC reprogramming from WT fibroblasts. Principal component analysis (PCA) mapped samples in a trajectory that reflects the progression of reprogramming from MEF to iPS/ES (Fig. 1H). MEF samples of all systems are clustered together in close proximity to WT samples measured in days 2, 4, 6 and 8, emphasizing the fast kinetics of NuRD-depleted systems compared to WT systems. *Mbd3<sup>f/-</sup>* and *Gatad2a<sup>-/-</sup>* samples from the same time points are closely mapped in both dimensions (Fig. 1H). Importantly, although previously published data measured in WT MEF and iPS (Polo et al., 2012) is clustered together with our corresponding samples, all other samples, which were measured from sorted cells undergoing reprogramming, are positioned in clusters based on the marker used for sorting and not according to the reprogramming day (Fig. 1H). In addition, Thy1+, Thy1- and SSEA1+ WT pre-iPSC samples do not cluster with any of the samples from *Mbd3<sup>f/-</sup>* or *Gatad2a<sup>-/-</sup>* systems beyond day 3 of reprogramming (PC1), possibly consistent with the notion that reprogramming measurements on inefficient stochastic reprogramming systems focus on early time points and infer data on populations most of which are not proceeding toward iPSCs.

Previous analysis on stochastic reprogramming systems have indicated two waves of major transcriptional changes, one at the beginning and the other at the end of iPSC

reprogramming, while in between there are very minor changes in transcriptional patterns (Hussein et al., 2014; Polo et al., 2012). We set out to test whether highly efficient reprogramming systems will show a similar pattern. 8,705 genes (of which 8,042 are polyA<sup>+</sup>) were identified as differentially expressed along the Mbd3<sup>f/-</sup> MEF to naïve iPSC 8-day reprogramming course (Table S3). These genes show a sequential activity, and can be sorted according to their expression temporal pattern, showing a continuous dynamic transition from the somatic program to the pluripotent one. Three major expression shifts are observed during the continuous dynamic transition (Fig. 1I): First, a large group of genes which are active in MEFs are down regulated as early as day 1. The second is a transient activation of genes between days 1 and 4. Finally, there is a gradual establishment of iPS/ES signature starting at day 5. Functional enrichment analysis in a single day resolution (Fig. 1I) characterized these changes: genes which are active in MEF and downregulated after DOX induction are enriched for somatic program processes (e.g. developmental process). Genes induced between days 1 and 6 are enriched for processes related to biosynthetic pathways (DNA and purine biosynthesis, translation). These processes are followed by induction of genes enriched for epigenetic remodeling and DNA repair processes. Finally, at day 6 there is a prominent induction of pluripotency maintenance master regulators including Nanog and Prdm14 (Fig. S1B). In summary, at the transcriptional level, during conducive reprogramming trajectory, somatic cell repression and pluripotency gene reactivation associated changes do not occur simultaneously and are separated in time. However, many other changes related to cellular adaptation occur in between, thus rendering global transcriptional changes rather continuous and not confined only to early and late stages of iPSC reprogramming (Fig. S2C-D; Table S4).

### Dynamic OSK binding governs conducive iPSC formation

We identified 40,174 enhancers with a dramatic change in activity, which is consistent between the two NuRD depletion approaches used (Fig. S2). We observed dynamic binding pattern for OSK in enhancers (Fig. 1D), which is changing during reprogramming from an early pattern to late pluripotency related pattern (Fig. 2A-C). cMyc has a strong preference to bind promoters over enhancers during reprogramming (Fig. 2B,D). Inspecting the binding co-localization of OSKM shows a clear difference between promoters and enhancers. Oct4-binding enhancers overlap with Sox2 and to a lesser extent with Klf4 targets throughout the process (Fig. 2D). The average probability to see co-localization of Oct4 and Sox2 in enhancers is 0.61 while in promoters it decreases to 0.39. However, the probability of Oct4 and Klf4 co-localization in promoters is higher by ~20% compared to enhancers. Differences between binding of enhancers and promoters are also apparent at the DNA motif level (Fig. 2E). While OSK-binding promoters are enriched mainly for temporally stable OSK binding motifs, OSK-binding enhancers are enriched for many additional and temporally varying binding motif patterns (Fig. 2E). This change in motif preference may indicate a change in the collaborative binding of OSK during reprogramming (Chronis et al., 2017), and may be responsible for the more dramatic changes in enhancer activity (5-fold increase in total differential enhancers (40,174 in comparison to differential gene promoters (8,042) underscores the magnitude of enhancer reprogramming).

We next asked if OSK are directly responsible for the repression of the somatic program. When inspecting enhancers that are active in MEF and repressed already at day 1, we observed that they are not significantly bound by OSK at any stage (not even when OSK are already expressed at day 1) (Fig. 2B). This observation is different from that previously reported (Chronis et al., 2017), who observed predominant OSK binding on MEF open enhancers at day 2 of the process. This difference is likely due to their usage of a system with <1% iPSC efficiency (Carey et al., 2010). Our observations and others who used highly efficient systems (Li et al., 2017) suggest that different regulators may mediate the repression of MEF-enhancers during successful reprogramming. Indeed, MEF-enhancers are enriched for binding motif of Runx1, Tead, Nf1 and Erg (p-val <math>10^{-70}</math>, Fig. S5F), and to much lower extent to Oct4 or Sox2 (p-val =

It has been previously shown that Oct4 and Sox2 are pioneer factors which have the ability to bind closed chromatin and to activate new regulatory elements. Specifically, 70% of the enhancers bound by OSK after 48h of reprogramming are in a closed chromatin state in human fibroblasts (Soufi et al. 2015). In the highly efficient mouse system used here, out of the 4,858 enhancers that are bound by OSK on day 1, 74% were in a closed state (no mark) in MEF and 4% were repressed by either H3K9me2 or H3K27me3. Further, when we examined the binding motifs abundant in closed vs. opened binding sites of OSK in day 1 of Mbd3<sup>f/-</sup> system, the canonical TF binding motifs of OSK were detected after 1 day of DOX induction in Mbd3<sup>flox/-</sup> cells in both closed and open regions (Fig. 2G). The latter is consistent with a pioneer TF activity for OSK in both mouse and human.

### Early enhancer demethylation marks commissioning of conducive reprogramming

We observed a global reduction in DNA methylation (Fig. 3A, S3A), which reaches its lowest level at day 8. We clustered enhancers based on their methylation levels (Fig. 3B). All 8 clusters showed different variations of progression exclusively entailing loss of DNA methylation, and none of the clusters showed continuous increase in methylation levels during the 8 days of reprogramming. The latter indicate that *de novo* DNA methylation is neither required for highly efficient and conducive iPSCs reprogramming and nor for repression of somatic lineage genes in naïve pluripotency reprogramming conditions (Lee et al. 2016, Polo et al., 2012).

We wanted to test whether different rates of demethylation exist for certain gene groups. We considered genes that are methylated in MEF (>80% methylation), and compared those that change their expression (FC>4) to those that do not change their expression (FC<1.5, Fig. 3C). We found that genes which are upregulated at some point during the process, undergo significantly faster demethylation compared to the non-changing genes, starting from day 6 following OSKM induction. When examining the methylation of enhancers (Fig. 3B) we identified one cluster (number 8), which is 68% methylated in MEF, and then undergoes fast demethylation (with average 43% methylation level on day 3), even before introducing 2i at day 3.5. The enhancers in this cluster are accessible between days 2 and 8, are highly

enriched for the binding of OSK (Fig. 3D), and highly overlap ( $p < 10^{-43}$ ) with ESC super-enhancers including Mir290, Tfap2c and Prdm14, which are known to boost iPSC efficiency (Table S5). Another cluster of enhancers (cluster 7) is enriched for SK binding and for ESC super enhancers, but it undergoes a slightly slower demethylation than cluster #8 (with average methylation of 67% in day 3), and its enhancers are accessible as measured by ATAC-seq only from day 6 until iPSC/ES (Fig. 3D). Both clusters are enriched for binding by Esrrb, E2f1, Klf4, but only cluster number 8 is enriched for Nanog and Oct4 binding.

We next aimed to unravel the mechanism underlying these different demethylation rates in our system and whether this early demethylation is important for achieving efficient reprogramming. Given that this demethylation occurs before introducing 2i we suspected that Tet enzymes, known to target and demethylate key pluripotency genes in ESC, might regulate this change. To test this, we established Tet1/2/3 triple floxed conditional knockout mouse model, from which we derived secondary iPSCs, generated isogenic *Gatad2a*<sup>-/-</sup> iPSC lines with CRISPR/Cas9 and subsequently re-isolated DOX inducible reprogrammable MEFs (Fig. 3E). Depletion of Tet enzymes in *Gatad2a*-WT decreased iPSC efficiency (from 32% to 6%). However, upon ablation of Tet enzymes in the *Gatad2a*<sup>-/-</sup> deterministic reprogramming system, reprogramming efficiency dropped from 93% down to 6-18%, similar to that in WT system, thus abolishing the beneficial effect of *Gatad2a* depletion (Fig. 3E). The latter indicate that Tet activity early in reprogramming is essential for highly efficient conducive iPSC reprogramming in NuRD depleted systems. Knockdown of Tfap2c or Tfcp2l1 reduced reprogramming efficiency by 15% (Fig. S3C). The latter suggests that early demethylation of selected enhancers by Tet enzymes promotes the commissioning of several pro-reprogramming factors that synergistically contribute to highly efficient reprogramming.

We tested whether the rapid demethylation of cluster 8 super-enhancers specifically detected during deterministic iPSC reprogramming, but not in bulk WT reprogramming samples (Fig. 3B), can be used as an early marker to prospectively enrich for the rare correctly commissioned WT cells to become iPSCs. To isolate cells in real time during reprogramming based on their DNA methylation status of a certain locus and at the single cell level, we utilized a recently generated reporter system for endogenous genomic DNA methylation (RGM) (Stelzer et al., 2015). We chose a validated RGM construct for Mir290 enhancer encoding tdTomato (RGM-SE-miR290-tdTomato), which was enriched in cluster 8, and introduced it in two OKSM DOX inducible reprogramming systems carrying Nanog-GFP reporter (Fig. 3F). In these inefficient WT systems, the first Nanog-GFP<sup>+</sup> cells appeared at days 10-14 following DOX induction, which were sorted and plated as single cells in naïve ESC media with or without continued DOX. As expected, over 90% iPSC efficiency was obtained following sorting Nanog-GFP<sup>+</sup> cells irrespective to the continued use of DOX to induce transgenes after sorting (Fig. 3F), confirming that Nanog-GFP<sup>+</sup> cells are already bona fide committed iPSCs that no longer need OSKM transgene expression. On the contrary, SE-miR290-tdTomato<sup>+</sup> cells appeared at very low frequency already at day 4 during reprogramming of *Mbd3/Gatad2a*-WT cells as single positive tdTomato<sup>+</sup> cells (Fig. S3B). tdTomato<sup>+</sup>/GFP<sup>-</sup> cells at day 5 were sorted and plated as single cells in naïve ESC media with or without continued DOX treatment. Remarkably, >85% iPSC efficacy, as measured by Nanog-GFP, was obtained from day 5 sorted tdTomato<sup>+</sup>/GFP<sup>-</sup> cells only upon



continued DOX supplementation (Fig. 3F). In the absence of continued DOX, 26% efficiency was obtained from early tdTomato+/GFP- sorted cells, suggesting that the sorted tdTomato+/GFP- cells are not bona fide iPSCs, however they were correctly “commissioned” and become committed to becoming iPSCs if OSKM expression is continuously delivered to drive the process toward completion. Day 5 double negative sorted cells did not yield any iPSCs after 10 days of DOX induction, indicating that this fraction marks somatic cells that did not optimally embark on a conducive trajectory towards becoming iPSCs. These results indicate that early demethylation of Mir290 super-enhancer marks correctly commissioned NuRD-WT somatic cells following DOX induction, that rapidly assume a conducive trajectory to becoming iPSCs if OSKM induction is continued. This also provides a means for early prospective isolation of adequately commissioned somatic cells for a successful reprogramming trajectory based on endogenous epigenetic feature.

### **Two synergistic and distinctly regulated gene programs ignite deterministic reprogramming**

We next wanted to characterize the epigenetic changes and examine their connection to the changes in gene expression. For each differentially expressed gene that showed a significant epigenetic modification in its promoter ( $n=7,801$ ), we calculated the correlation between its transcriptional temporal pattern and chromatin modification patterns, measured around the transcription start site or transcription end site (TSS and TES, respectively) across all time points. When we cluster these genes and chromatin marks (Fig. 4A), we observed that chromatin marks separate into two clusters: One consists of marks which are positively correlated to gene expression, and are indeed known to be associated with active transcription, such as H3K4me3, H32K7Ac, H3K36me3 (in TES) and chromatin accessibility. The other consists of marks which negatively correlate with gene expression, and are known repression-associated marks, such as H3K27me3 and H3K9me3. Interestingly, the genes also separate into two main clusters. One consists of genes that display high correlation (positive or negative) between expression and chromatin modifications, and the other consists of genes that are not correlated, despite the fact that the genes are differentially expressed. Notably, each of these two gene groups contains both induced and repressed genes (Fig. S4A-B). We inspected the actual transcriptional and epigenetic patterns for these two gene clusters, focusing on H3K27ac and H3K27me3 marks, which showed the highest positive and negative correlation to transcription (Fig. 4B). The genes in the first group showed a clear switch-like behavior between the epigenetic marks (Fig. 4B, S4A), correlated with the activation or repression. We therefore concluded that these are genes with Epigenetically Switched Promoters (abbreviated as ESPGs). In the second group, the majority of the genes ( $N=3049$ , 72%) had differential transcription (above 4-fold change), but with consistently high levels of H3K27ac and low levels of H3K27me3 ( $z$ -score  $<0.7$ , Fig. 4B, S4B). The promoters of these genes show a constitutive active chromatin signature, suggesting that these genes are regulated by distinct mechanisms. We refer to this group as CAPGs (Constitutively Active Promoter Genes) (Table S6). In accordance with chromatin modifications, DNA methylation in the promoters and enhancers of the two groups is different (Fig. S4C-D): CAPGs show a consistent hypomethylation,

regardless of their transcriptional pattern, whereas ESPGs, which are regulated on the chromatin level, are also regulated by DNA methylation.

Inspecting the functional enrichment of the two groups, we found a specific association of ESPGs to cell fate determination processes, indicating that epigenetic regulation is highly specific for cell fate genes. CAPGs are enriched for biosynthetic pathways including DNA synthesis, proliferation, DNA repair and chromatin reorganization (Fig. 4C). The two programs show a distinct conservation pattern during the evolution of vertebrate organisms: while in vertebrates CAPGs and ESPGs are conserved in a similar degree (Fig. 4F), in fungi and other non-vertebrates CAPGs are more conserved than ESPGs ( $p < 10^{-30}$ ), emphasizing their basic role in cellular maintenance. The two groups also show distinct regulation by c-Myc: CAPGs, but not ESPGs, are significantly bound by c-Myc (sample median  $p < 10^{-75}$  for CAPGs, sample median  $p > 0.9$  for ESPGs) (Fig. 4D). This is supported also by over representation of c-Myc motif only in CAPGs promoters (Fig. 4C). Additional TF binding motifs show enrichment specific to one group and not the other (Fig. 4C), further supporting a model of separate regulation. Finally, the two groups have different temporal behavior: while ESPGs have a gradual change in activity along reprogramming, CAPGs converge to their final activity pattern as early as day 1 (Fig. 4B,E). Importantly however, these two programs retain a coupled and cross-coordinated regulation. Protein binding enrichment in ESPGs and CAPGs using public protein-DNA databases shows a number of proteins that are associated with one of the groups, but bind the opposite group. Several epigenetic modifying components such as Polycomb and Wdr5, that show a constitutively active promoter configuration, but regulate ESPGs (Fig. 4G).

### Two divergent modes of epigenetic repression of ESPGs

We next sought to discern epigenetic regulation during iPSC formation, and from the differentially expressed genes we focused on ESPGs as they are the ones that undergo a repressive to activation switch or vice versa. We used the chromatin modification coverage in promoters and the RNA expression level, and calculated the temporal correlation distribution for all ESPGs (Fig. 5A), i.e. correlation that is calculated for each gene, over all time points. RNA-PolIII, H3K27ac and H3K4me3 in promoters are highly correlated to gene expression of the genes they decorate (Median  $r = 0.55, 0.7, 0.6$ , respectively). H3K27me3, H3K9me2 and H3K9me3 show negative correlation to gene expression. Examining the frequencies of combinations of chromatin modifications (Fig. 5B) on gene promoters, we observed that in upregulated ESPGs ( $n = 431$ ), there is a rapid reduction of H3K9me2 and H3K27me3. In addition, there is a substantial increase in H3K27ac and binding of PolIII, such that by day 8 and iPSC, 45% of the promoters are decorated by the combination of H3K27ac and PolIII. In the downregulated ESPGs ( $n = 974$ ), we observe the opposite pattern with loss of H3K27ac and PolIII binding, and gain of H3K27me3 starting from day5 (Fig. 5B).

The analysis above also highlights the most frequent combinations, and the combinations that are not apparent in the data and are mutually exclusive. The latter allowed us to ask whether mutually exclusive modes of repression exist in iPSC reprogramming. Active marks (H3K27ac, RNA-PolIII, ATAC) tend to appear together on promoters (Fig. 5B), and we did



not discern distinct mutually-exclusive modes of acquiring activation marks. On the contrary, repressive marks (H3K27me3, H3K9me2) work separately from one another. We observed that less than 1% of the promoters are marked by both H3K9me2 and H3K27me3, suggesting these are mutually exclusive marks. Indeed, our data show a clear association between H3K9me2 and DNA methylation (Fig. S15A) and this may explain why in our system, which undergoes substantial DNA demethylation, there is a limited gain of H3K9me2 on downregulated ESPGs. Furthermore, H3K27me3 decorates genes that are enriched for functions in development, while H3K9me2 decorates genes related to signaling pathways (Fig. 5B). H3K27me3 genes are naturally highly enriched for Polycomb targets (Fig. S5B), and an induction in the expression of Polycomb members is observed, which overlaps with the increase in H3K27me3 peaks starting from day 5 (Fig. 5B). Altogether, this analysis uncovers two divergent modes of epigenetic repression by H3K27me3 and H3K9me2 during iPSC reprogramming with opposing association with DNA methylation and distinct associated regulatory functions.

Bivalent promoters, which carry both H3K27me3 repressive mark and H3K4me3 active mark, constituted 38% of ESPGs and were found to constitute a third distinct mode of repression (Fig. 5B, S5F). Bivalent promoters are highly enriched for developmental regulators (Fisher exact test  $p\text{-val} < 10^{-90}$ , FDR corrected), and overlap with bivalent promoters that were detected previously in MEFs and in ESCs (Fig. S5B). When comparing bivalent promoters to H3K27me3-only promoters we observe that the repression of transcription is stronger in H3K27me3-only promoters than in bivalent ones (One tailed Wilcoxon test,  $p\text{-value} < 10^{-98}$ ). Moreover, the chromatin of bivalent promoters is much more accessible compared to H3K27me3-only or to H3K9me2 promoters, which decorate closed chromatin (Fig. S5C-F). To rule out the possibility that bivalent signature is a mere result of a residual mixed cell population in the highly efficient system, we note that other combinations that are mutually exclusive in promoters, such as H3K27me3 and H3K27ac, appear in much lower frequency (<3%) compared to the bivalent combinations (>25%).

### **Repressive and active chromatin mark switching are temporally separated over ESPGs**

The temporal interplay between the different chromatin marks remains to be defined at high-resolution, and it is unclear whether during transitions from repressed to activated state changes in repressive and activating epigenetic modes co-occur simultaneously or are well separated. Since our data consist of time-series we used Cross Correlation, a signal-processing algorithm widely used to detect and quantify the temporal offset between signals (Kiviet et al., 2014) (Fig. S6), to test whether the deposition of these modifications has a temporal order. We estimated the distribution of offsets across ESPGs (Fig. 5C), i.e., for each ESPG we calculate the cross-correlation between its temporal expression and the temporal pattern of each of the epigenetic marks, across MEF to iPSC samples. The analysis clearly highlighted separation between accumulation of repressive and activation marks at gene promoters. In induced genes, first, DNA is demethylated and H3K27me3 is removed, and only then chromatin becomes accessible. Finally, H3K27ac, RNA-PolIII and H3K4me3 accumulate in the promoter in a close proximity to transcriptional activation (Fig. 5C). The latter also excludes an alternative scenario wherein gene activation, removal of repressive marks follows epigenetic activation and transcription initiation (Fig. 5C). In repressed genes,

PolII disassociates from its bound promoters in close proximity to the eviction of H3K27ac and H3K4me3 and chromatin closure (Fig. 5C). Only afterwards, repressive marks like H3K27me3 and H3K9me3 gradually accumulate during the following days.

Our next aim was to elucidate the temporal order of epigenetic changes that occur in differential enhancers and how they compare to those observed in promoters. 43% of all annotated enhancers (n=40,174) showed differential ATAC-seq and H3K27ac signals in both *Mbd3<sup>f/-</sup>* and *Gatad2a<sup>-/-</sup>* systems, and were identified as differential enhancers (Fig. S2A). The enhancer activation kinetics in the two NuRD depleted systems were highly consistent and faster than the WT systems (Fig. S4B-D). We calculated the correlation between chromatin accessibility and chromatin modification in each of the differential enhancers (Fig. 5D), and observed positive correlation with H3K27ac modification (median  $r=0.55$ ). Interestingly, positive correlation was evident between enhancer accessibility and RNA-PolII binding. Furthermore, we observed negative correlation between enhancer accessibility and DNA-methylation, H3K27me3 and H3K9me2, but to less extent with H3K9me3 modification. H3K27me3 does not always decorate repressed enhancers. In fact, when all possible combinations of chromatin marks are inspected in differential enhancers (Fig. 5E), 85% of the enhancers which are active in day 8 are in a closed chromatin state on day 0 (MEF), but are not marked by any of the histone marks measured herein. Like in promoters, H3K9me2 repression can be observed in the first days of reprogramming, is later depleted, and is mutually exclusive to H3K27me3 (Fig. 5E). Unlike its abundance on promoters during reprogramming, bivalency at enhancers (H3K27me3 with H3K4me1) is rare, and H3K27me3 is rarely deposited on accessible enhancers (<4%, Fig. 5E, S5E).

To examine the sequence of epigenetic events during enhancer activation and suppression, we used Cross-Correlation and quantified the temporal offset between chromatin changes and DNA accessibility in each differential enhancer. We found that in activated enhancers (n=17,174), H3K27me3 is first removed, then H3K4me1 is deposited, followed by chromatin accessibility and deposition of H3K27ac and finally, by binding of RNA-PolII (Fig. 5F). In repressed enhancers, PolII release and the removal of H3K27ac and H3K4me1 happen all in close proximity to chromatin closure timing, followed by gradual deposition of H3K27me3 or H3K9me2. Thus overall, the orderly switches from activation to repression (or vice versa) over enhancers are similar to those seen over promoters (Fig 5C,F). Cross-Correlation was used to quantify the temporal order of epigenetic changes in enhancers and promoters in relation to measured transcription changes (Fig. S7A). No significant temporal differences were observed in deposition or removal of repressive chromatin marks between enhancers and promoters during repression or activation of ESPGs, respectively (Fig. S7A). However, we could see that active modifications are deposited on enhancers before they are deposited on the associated promoters during gene activation (paired sample t-test ATAC-seq  $p<10^{-7}$ , H3K27ac  $p<10^{-11}$ , H3K4me3  $p<10^{-2}$ , respectively). In contrast, during ESPG repression, eviction of activation marks on enhancers was significantly lagging in comparison to promoters (Fig. S7A). Unexpectedly, RNA-PolII binds enhancers and showed similar behavior to the activating epigenetic marks (PolII binds enhancers slightly before it binds to promoters ( $p<10^{-3}$ , Fig. S7A-C) and leaves the enhancers slightly after it leaves the promoters ( $p<10^{-23}$ ))<sup>52</sup>. RNA-PolII binding in enhancers is highly correlated both to gene

transcription (Fig. S7D) and to enhancer activity (Fig. 5D). Independent RNA-PolII binding data, measured in mouse ESC (Rahl et al., 2010), was also highly enriched among enhancers which are active in late reprogramming stage ( $p < 10^{-200}$ , Fig. S7B). These results indicate that the phenomenon of PolII recruitment to enhancers as an early event of enhancer commissioning, is widely abundant during iPSC reprogramming.

### **Myc activity is essential for iPSC reprogramming**

CAPGs are predominantly regulated by Myc and drive cellular biosynthetic processes. As exogenous Myc is dispensable for iPSC formation from WT and NuRD-depleted somatic cells (Nakagawa et al., 2008), this raised the possibility that the observed CAPGs induction is a side-effect of c-Myc over-expression and is not essential for the reprogramming process. To test this, we introduced perturbations to the highly efficient optimally NuRD-depleted reprogramming protocols.

First, we tested reprogramming with a viral induction of only 3 factors OSK (Fig. 6A (i)). Notably, CAPGs that were upregulated in the original protocol, were still significantly upregulated compared to MEF ( $P\text{-val} < 10^{-12}$ , Fig. 6B). However, we noticed that in OSK reprogramming, endogenous c-Myc continues to be highly expressed and endogenous n-Myc is induced after OSK induction ( $FC > 1.8$ , for both c-Myc and n-Myc). We tested OSK reprogramming under inhibition of endogenous Myc family members by treating MEFs that carry OSK cassette with siRNAs for c-Myc, n-Myc and l-Myc starting on day -3 prior to DOX induction (Fig. 6A (ii)). Myc inhibition resulted in dramatic reduction in reprogrammed colonies (Fig. 6C,D). The downregulation and upregulation of ESPGs was also diminished by Myc inhibition (Fig. 6E), although Myc does not bind them directly (Fig. 4); suggesting that this change is caused indirectly. We used conditional knockout fibroblasts for both c-Myc and n-Myc genes and carrying *Lox-stop-Lox-YFP* reporter in the *Rosa26* locus which can mark floxed cells upon Cre-treatment. Fibroblasts were treated with CAGGS-Cre plasmid, sorted for YFP and subjected to either OSK or OSKM transduction (Fig. 6F). Remarkably, we could not obtain any YFP+ iPSC colonies following OSK induction and follow up of over 30 days of reprogramming from Cre-treated cells (Fig. 6G). Following applying MYC inhibition during the first 4 days of reprogramming by in secondary *Mbd3<sup>fllox/-</sup>* cells, we noted that downregulation of somatic marker *Thy1*, one of the earliest events in MEF reprogramming, is abrogated (Fig. 6H). These findings show that there is no initiation of reprogramming process in the absence of Myc activity and reveals an early critical role for MYC in conducive iPSC formation. Inhibition of MYC activity abolished highly efficient B cell reprogramming by C/EBPa+OSKM, mouse common myeloid progenitors and human iPSC reprogramming by OSK (Fig. 5U-J). The latter findings are consistent with the high similarity and convergence in gene expression and accessibility changes found in our NuRD depleted MEF systems and that in highly efficient B cell to iPSC reprogramming (Fig. 2H, S2E-F).

Molecularly, c-Myc over-expression (OE) in MEF, without the induction of other reprogramming factors, induced CAPGs expression changes in the same way it changes during reprogramming by OSKM (Fig. 6B), also causing significant repression of downregulated ESPGs (somatic genes), but did not lead to the induction of upregulated

ESPGs (pluripotency genes). We further validated Myc induced CAPG changes by looking at specific functional groups of genes: Genes related to cell biosynthesis, which are bound by c-Myc (Fig. 6K,L) are induced upon overexpression of c-Myc. These expression changes are consistent with previously published data (Scognamiglio et al., 2016) of Myc inhibition and reconstitution measured independently during naïve mouse ESCs maintenance (Fig. 6M). Interestingly, we observed that reprogramming related chromatin modifiers such as Prc2 members, Tet1, Wdr5 are induced by the mere OE of c-Myc, and fail to be induced upon its inhibition (Fig. 6N). This indicates that Myc has a critical role in igniting the biosynthetic pathways that are dispensable for pluripotency maintenance (Scognamiglio et al., 2016), yet essential for reestablishing pluripotency in somatic cells and must be provided either endogenously or exogenously.

### Rapid rewiring of tRNA pool boosts Myc dominated CAPG

The rapid change in CAPGs expression, without associated changes in their epigenetic signature, raised the possibility that CAPGs may be differently regulated. A recent study (Gingold et al., 2014) documented a cancer promoting mechanism that supports loss of somatic identity and acquisition of a highly active metabolic state during cancer transformation involving coordinated changes in the tRNA pool and the codon usage preference of tRNA. We thus examined if such shifts occur at the codon usage level of the transcriptome and at tRNA transcription status when somatic cells undergo reprogramming toward pluripotency. To characterize putative changes in the codon usage of the transcriptome, we calculated the average codon usage distribution of all differential genes in the four reprogramming systems. Using PCA we characterized the codon combination that shows the highest variability during reprogramming (Fig. 7A) and noticed a change in codon combination that separates between early and late stages of reprogramming. The observed change in codon usage corresponds to a shift from G/C-ending codons to A/T-ending codons (Fig. 7B), with the most prominent change occurring already at the first day of reprogramming of NuRD depleted, but not WT cells. We characterized the codon combination that shows the highest variability, for each subset of ESPGs, CAPGs, or total differential genes (Fig. 7C,D). Surprisingly, the codon usage in ESPGs (red) and CAPGs (green) clustered at the lower and upper margins of the first principle component, respectively. The latter showed divergence in codon usage programs between the CAPGs and ESPGs: while ESPGs mainly tend to use codons that end with a G/C at the third codon position, CAP genes split into two programs: the genes that are induced during reprogramming, are encoded with A/T ending codons, while those that are repressed in the process mainly use G/C-ending codons (Fig. 7C,F). Interestingly, we did not see any significant change in codon usage when comparing different time points of ESPGs, but we do see a rapid and significant change in codon usage of CAPGs already emerging already between day0 and day1 (Fig. 7C) which underlies the global change observed during reprogramming.

The efficiency of translation elongation is determined by the relation between the supply of tRNAs and the demand for specific tRNA types, governed by the representation of the 61 sense codons in the transcriptome. We asked whether the changes in codon usage along reprogramming are accompanied with a coordinated change in the tRNA pool. We measured

the chromatin mark H3K4me3 in the vicinity of the tRNA genes, and observed a change in tRNA expression throughout reprogramming (Fig. 7G). We next asked whether the change in the tRNA pool along reprogramming correspond to the observed change in the codon usage of the translated transcriptome, and calculated the expected translational efficiency for genes belonging to the most highly enriched GO categories corresponding to up/down regulated ESPGs and CAPGs based on their codon sequence and the tRNA epigenetic status. We observed a global significant positive correlation between the changes in transcription and translation, suggesting that the anticodons whose expression is elevated along reprogramming correspond to the codons that are enriched in the transcriptome of the respective cell state (Spearman  $r = 0.45$ ,  $p < 4.5e-49$ , Fig. 7H). However, while GO annotations that are associated with upregulated CAPGs showed an increase in translation efficiency (Fig. 7I), GO annotations associated with upregulated ESPGs show an opposite trend: a decrease in translation efficiency, corresponding to their G/C-ending codon preference (Fig. C-D). Thus, the CAPG program is responsible for biosynthetic processes and is optimally boosted by Myc and tRNA codon usage.

## Star \* Methods

Key Resources Table

REAGENT or RESOURCE	SOURCE	IDENTIFIER
<b>Antibodies</b>		
H3K4Me1	Abcam	Cat# ab8895; RRID:AB_306847
H3K4Me3	Abcam	Cat# Ab8580, RRID:AB_306649
H3K27ac	Abcam	Cat# ab4729, RRID:AB_2118291
H3K27Me3	Millipore	Cat# 07-449, RRID:AB_310624
H3K9Me3	Abcam	Cat# ab8898, RRID:AB_306848
H3K36Me3	Abcam	Cat# ab9050, RRID:AB_306966
H3K9Me2	MBL	Cat# MABI0317, RRID: N/A
Oct4	Santa Cruz	Cat# SC8628, RRID:AB_653551
Klf4	R&D	Cat# AF3158, RRID:AB_2130245
Sox2	Millipore	Cat# AB5603, RRID:AB_2286686
C-Myc	Santa Cruz	Cat# sc764, RRID:AB_631276
PolII (N20)	Santa Cruz	Cat# sc899, RRID:AB_632359
<b>Chemicals, Peptides, and Recombinant Proteins</b>		
PD0325901	Axon Medchem	1408
CHIR99021	Axon Medchem	#1386
Recombinant human LIF	Peptotech	300-05
c-Myc inhibitor 10058-F4	Axon Medchem	#2222
cOmplete, Protease inhibitor	Roche	04693159001
Protease inhibitor cocktail (Sigma)	Sigma-Aldrich	P8340
<b>Critical Commercial Assays</b>		
Alkaline Phosphatase Kit	Millipore	SCR004

REAGENT or RESOURCE	SOURCE	IDENTIFIER
Lipofectamine RNAiMAX	ThermoScientific	#13778075
TruSeq RNA Sample Preparation Kit v2	Illumina	RS-122-2001
EZ DNA Methylation-Gold kit	Zymo	D5005
EpiGenome Methyl-Seq	Illumina	EGMK81312
Truseq small RNA sample preparation kit	Illumina	RS-200-0012
<b>Deposited Data</b>		
ATAC-Seq, ChIP-Seq, RNA-Seq, WGBS	This Paper	GSE102518
<b>Experimental Models: Cell Lines</b>		
<i>Mbd3</i> <sup>flox/-</sup> cell lines that carries the GOF18-Oct4-GFP transgenic reporter, FUW-M2RtTA; FUW-TetO-STEMCCA-humanOKSM – ES and Secondary MEF	Rais et al. (2013)	N/A
RGM-miR290-SE-tdTomatom Nanog-GFP	Stelzer et al. (2015)	N/A
FUW-M2RtTA; FUW-TetO-STEMCCA-humanOKSM, PE-GOF18-Oct4-GFP cells (Both Gatad2a WT and KO)	Mor et al. (2018)	N/A
Tet1,2,3 <sup>ff</sup> MEF and iPSC cell line	This paper	N/A
c-Myc <sup>ff</sup> , n-Myc <sup>ff</sup> Rosa26-Lox-stop-Lox-YFP	Scognamiglio et al. (2016)	N/A
V6.5 murine ESC line	Beard et al. (2006)	N/A
<b>Experimental Models: Organisms/Strains</b>		
Tet2 <sup>flox/flox</sup> (B6;129S-Tet2tm1.1Haai/J) mouse strain	Jackson	# 017573, RRID:IMSR_JAX:017573
Tet1,2,3 flox/flox	This paper	N/A
<b>Oligonucleotides</b>		
siRNA targeting Mouse-cMYC	Invitrogen	MSS-237326, MSS-237327, MSS-237328
siRNA targeting Mouse-IMYC	Invitrogen	MSS-275360, MSS-275361, MSS-275362
siRNA targeting Mouse-nMYC	Invitrogen	MSS-207081, MSS-207082, MSS-276042
Stealth RNAi <sup>TM</sup> siRNA Negative Control, Med GC	Invitrogen	12935300
siRNA targeting Mouse Tfp2c	Invitrogen	MSS-210701, MSS-277866, MSS-277867
siRNA targeting Mouse Bend3	Invitrogen	MSS-221180, MSS-221181, MSS-221182
siRNA targeting Mouse Tfc211	Invitrogen	MSS-294469, MSS-294470, MSS-294471
<b>Recombinant DNA</b>		
pLM-mCerulean-cMyc	Addgene	Addgene #23244
FUW-M2rtTA	Addgene	Addgene #20342



REAGENT or RESOURCE	SOURCE	IDENTIFIER
FUW-TetO-STEMCCA-humanOKS-mCherry	Mor et al. (2018)	N/A
FUW-TetO-STEMCCA-humanOKSM	Mor et al. (2018)	N/A
<b>Software and Algorithms</b>		
Tophat 2.0.10	<a href="https://ccb.jhu.edu/software/tophat/index.shtml">https://ccb.jhu.edu/software/tophat/index.shtml</a>	<a href="https://ccb.jhu.edu/software/tophat/index.shtml">https://ccb.jhu.edu/software/tophat/index.shtml</a>
Cufflinks 2.2.1	<a href="http://cole-trapnell-lab.github.io/cufflinks/">http://cole-trapnell-lab.github.io/cufflinks/</a>	<a href="http://cole-trapnell-lab.github.io/cufflinks/">http://cole-trapnell-lab.github.io/cufflinks/</a>
R pheatmap package	<a href="https://cran.r-project.org/web/packages/pheatmap/index.html">https://cran.r-project.org/web/packages/pheatmap/index.html</a>	<a href="https://cran.r-project.org/web/packages/pheatmap/index.html">https://cran.r-project.org/web/packages/pheatmap/index.html</a>
R prcomp package	<a href="https://stat.ethz.ch/R-manual/R-devel/library/stats/html/prcomp.html">https://stat.ethz.ch/R-manual/R-devel/library/stats/html/prcomp.html</a>	<a href="https://stat.ethz.ch/R-manual/R-devel/library/stats/html/prcomp.html">https://stat.ethz.ch/R-manual/R-devel/library/stats/html/prcomp.html</a>
Bowtie 2	<a href="http://bowtie-bio.sourceforge.net/bowtie2/index.shtml">http://bowtie-bio.sourceforge.net/bowtie2/index.shtml</a>	<a href="http://bowtie-bio.sourceforge.net/bowtie2/index.shtml">http://bowtie-bio.sourceforge.net/bowtie2/index.shtml</a>
Picard tools	<a href="http://broadinstitute.github.io/picard/">http://broadinstitute.github.io/picard/</a>	<a href="http://broadinstitute.github.io/picard/">http://broadinstitute.github.io/picard/</a>
MACS 1.4.2	<a href="http://liulab.dfci.harvard.edu/MACS/">http://liulab.dfci.harvard.edu/MACS/</a>	<a href="http://liulab.dfci.harvard.edu/MACS/">http://liulab.dfci.harvard.edu/MACS/</a>
bedtools	<a href="http://bedtools.readthedocs.io/en/latest/">http://bedtools.readthedocs.io/en/latest/</a>	<a href="http://bedtools.readthedocs.io/en/latest/">http://bedtools.readthedocs.io/en/latest/</a>
samtools	<a href="http://www.htslib.org/doc/samtools.html">http://www.htslib.org/doc/samtools.html</a>	<a href="http://www.htslib.org/doc/samtools.html">http://www.htslib.org/doc/samtools.html</a>
IGV	<a href="https://software.broadinstitute.org/software/igv/">https://software.broadinstitute.org/software/igv/</a>	<a href="https://software.broadinstitute.org/software/igv/">https://software.broadinstitute.org/software/igv/</a>
Python misha package	<a href="https://bitbucket.org/tanaylab/misha-package">https://bitbucket.org/tanaylab/misha-package</a>	<a href="https://bitbucket.org/tanaylab/misha-package">https://bitbucket.org/tanaylab/misha-package</a>
MATLAB	MathWorks	<a href="https://www.mathworks.com/products/matlab.html">https://www.mathworks.com/products/matlab.html</a>
Prism	GraphPad software	<a href="https://www.graphpad.com/scientific-software/prism/">https://www.graphpad.com/scientific-software/prism/</a>
FlowJo	FlowJo	<a href="https://www.flowjo.com/">https://www.flowjo.com/</a>
ZEN Software	Zeiss	<a href="https://www.zeiss.com/microscopy/int/products/microscope-software/zen-lite.html">https://www.zeiss.com/microscopy/int/products/microscope-software/zen-lite.html</a>
<b>Other</b>		

## Contact For Reagent and Resources Sharing

Further information, and requests for reagents will be fulfilled by the Lead Contact, Dr. Jacob H. Hanna ([Jacob.hanna@weizmann.ac.il](mailto:Jacob.hanna@weizmann.ac.il)).

## Experimental Model and Subject Details

### Mice

Tet2<sup>fllox/fllox</sup> mice were obtained from Jackson Laboratories (Stock number 017573). All animal experiments were performed according to the Animal Protection Guidelines of Weizmann Institute of Science, Rehovot, Israel. All animal experiments described herein were approved by relevant Weizmann Institute IACUC (#00330111-Hanna). All efforts were made to minimize animal discomfort.

## Cell Culture

WT or Mutant mouse ESC/iPSC lines and sub-clones were routinely expanded in mouse ES medium (mESM) consisting of: 500ml DMEM-high glucose (ThermoScientific), 15% USDA certified Fetal Bovine Serum (Biological Industries), 1mM L-Glutamine (Biological Industries), 1% nonessential amino acids (Biological Industries), 0.1mM  $\beta$ -mercaptoethanol (Sigma), penicillin-streptomycin (Biological Industries), 10 $\mu$ g recombinant human LIF (PeproTech). For ground state naïve conditions (N2B27 2i/LIF), murine naïve pluripotent cells (iPSCs and ESCs) were conducted in serum-free chemically defined N2B27-based media: N2B27-based media: 250ml Neurobasal (ThermoScientific), 250ml DMEM:F12 (ThermoScientific) 5ml N2 supplement (Invitrogen; 17502048), 5ml B27 supplement (Invitrogen; 17504044), 1mM glutamine (Invitrogen), 1% nonessential amino acids (Invitrogen), 0.1mM  $\beta$ -mercaptoethanol (Sigma), penicillin-streptomycin (Invitrogen), 5mg/ml BSA (Sigma), small-molecule inhibitors CHIR99021 (CH, 3  $\mu$ M - Axon Medchem) and PD0325901 (PD, 0.3-1  $\mu$ M - Axon Medchem). Mycoplasma detection tests were conducted routinely every month with MycoALERT ELISA based kit (Lonza) to exclude mycoplasma free conditions and cells throughout the study.

## Method Details

### Generation of *Gatad2a*-knockout Reprogrammable secondary MEF lines

Secondary MEF for *Gatad2a*<sup>-/-</sup> cell line and WT-2 were obtained as described in (Mor et al., 2018). Shortly, iPSCs were established following primary reprogramming of cells using M2rtTA and TetO-OKSM-STEMCCA (human OSKM cDNA inserts were used). The iPSC, harboring mCherry constitutive expression (to label viable cells) and PE-GOF18-Oct4-GFP cassette (Addgene plasmid# 52382), were then subjected to CRISPR/Cas9 targeting *Gatad2a* (sgRNA- cgctgatgtgattgtgct), resulting in *Gatad2a*-knockout cells (Mor et al., 2018). Both *Gatad2a*-KO and its isogenic wild-type line (WT-2) were then injected into blastocysts, and MEF were harvested at E13.5. MEFs were harvested at E13.5 and grown in MEF medium, which contained 500 ml DMEM (Invitrogen), 10% fetal calf serum (Biological Industries), 1 mM glutamine (Invitrogen), 1% non-essential amino acids (Invitrogen), 1% penicillin–streptomycin (Invitrogen), 1% sodium pyruvate (Invitrogen). All animal studies were conducted according to the guideline and following approval by the Weizmann Institute IACUC (approval # 33550117-2 and 33520117-3). Cell sorting and FACS analysis were conducted on 4 lasers equipped FACS Aria III cells sorter (BD). Analysis was conducted with either DIVA software or Flowjo. Throughout this study, all cell lines were monthly checked for Mycoplasma contaminations (LONZA – MYCOALERT KIT), and all samples analyzed in this study were never tested positive or contaminated.

### Generation of reprogrammable *Mbd3*<sup>fllox/-</sup> secondary MEF lines

All secondary reprogrammable lines harbor constitutive expression of the M2rtTA from the Rosa26 locus and TetO-OKSM cassette (human OKSM cDNA inserts were used) introduced either by viral transduction of knock-in in the *Col1a1* locus. Secondary mouse embryonic fibroblast (MEF) from *Mbd3*<sup>fllox/-</sup> cell line (A12 clone: *Mbd3*<sup>fllox/-</sup> cell lines that carries the GOF18-Oct4-GFP transgenic reporter (complete *Oct4* enhancer region with distal and proximal enhancer elements) (Addgene plasmid #60527)) and WT-1 cell line (WT-1 clone

that carries the deltaPE-GOF18-Oct4-GFP reporter (Addgene plasmid#52382) were previously described (Rais et al., 2013). Note that we do not use Oct4-GFP or any other selection for cells before harvesting samples for conducting genomic experiments.

### Mouse embryo micromanipulation

Pluripotent mouse ESCs and iPSCs were injected into BDF2 diploid blastocysts, harvested from hormone primed BDF1 6-week-old females. Microinjection into E3.5 blastocysts placed in M16 medium under mineral oil was done by a flat-tip microinjection pipette. A controlled number of 10-12 cells were injected into the blastocyst cavity. After injection, blastocysts were returned to KSOM media (Invitrogen) and placed at 37°C until transferred to recipient females. Ten to fifteen injected blastocysts were transferred to each uterine horn of 2.5 days post coitum pseudo-pregnant females.

### Reprogramming of MEF to naive ground state naive iPSC

Reprogramming of the optimally NuRD depleted and WT platform cell lines to iPSC was performed for the first 3 days with MES medium, which contained 500 ml DMEM (Invitrogen), 15% fetal calf serum, 1 mM glutamine (Invitrogen), 1% non-essential amino acids (Invitrogen), 1% penicillin–streptomycin (Invitrogen), 1% sodium pyruvate (Invitrogen), 0.1 mM  $\beta$ -mercaptoethanol (Sigma), 20 ng/ml human LIF (in house prepared). MES medium for reprogramming was supplemented with Doxycycline (DOX) (2  $\mu$ g ml<sup>-1</sup>), which activated the OKSM cassette and the reprogramming process. On day 3.5, medium was replaced to FBS-free media composed of: 500 ml DMEM (Invitrogen), 15% knockout serum replacement (Invitrogen; 10828), 1 mM glutamine (Invitrogen), 1% non-essential amino acids (Invitrogen), 0.1 mM  $\beta$ -mercaptoethanol (Sigma), 1% penicillin–streptomycin (Invitrogen), 1% sodium pyruvate (Invitrogen), 20 ng/ml recombinant human LIF (Peprotech or in house-prepared), CHIR99021 (3  $\mu$ M; Axon Medchem), PD0325901 (PD, 0.3-1  $\mu$ M; Axon Medchem). After DOX treatment medium was replaced to KSR-based with the addition of MEK and GSK3 inhibitors (2i), supplemented with Doxycycline (DOX) (2  $\mu$ g ml<sup>-1</sup>), until the end of the reprogramming regimen (i.e. day 8). Cells were harvested at first time point (MEF) and every 24 hours until day 8 and were used for library preparation followed by sequencing. *Mbd3<sup>f/-</sup>*, *Gatad2a<sup>-/-</sup>* and WT established iPSC line (after 3 passages or more), and *Mbd3<sup>f/-</sup>* or WT V6.5 mouse ESCs were used as controls. For all mouse iPSC reprogramming experiments, irradiated human foreskin fibroblasts were used as feeder cells, as any sequencing input originating from the use of human feeder cells cannot be aligned to the mouse genome and is therefore omitted from the analysis. All cell undergoing reprogramming were harvested without any prior passaging or sorting for any subpopulations during the reprogramming process. No blinding was conducted when testing outcome of reprogramming experiments.

### Primary and secondary reprogrammable lines by viral infection

For primary cell reprogramming,  $\sim 3 \times 10^6$  293T cells in a 10cm culture dish were transfected with JetPEI® (Polyplus) 20ul reagent for 10ug DNA as follow: pPAX (3.5  $\mu$ g), pMDG (1.5  $\mu$ g) and 5 $\mu$ g of the lentiviral target plasmid (pLM-mCerulean-cMyc (Plasmid #23244), FUW-STEMCCA-OKS-mCherry or FUW-M2rtTA, FUW-TetO-STEMCCA-OKS-mCherry (a kind gift from Gustavo Mostoslavsky). Viral supernatant was harvest 48 and 72 hours post

transfection, filtered through 0.45micron sterile filters (Nalgene) and added freshly to the primary MEF that was isolated from Mbd3<sup>flox/-</sup> chimeric mice (unless indicated otherwise). At day 4 cells was sorted by the relevant florescent filter (mCerulean (cMyc OE), mCherry (OSK OE) or double positive (OSK+M OE) cell was collected for RNA extraction or seeded for farther growth.

### Knockdown endogenous Myc during reprogramming

For secondary Mbd3<sup>flox/-</sup> OSK<sup>2nd</sup> production, primary MEFs from Mbd3<sup>flox/-</sup> chimeric mice were infected with FUW-TetO-STEMCCA-OKS-mCherry and FUW-M2rtTA. iPS cells were isolated and injected into BDF2 blastocysts for the isolation of secondary MEFs. Secondary MEFs were transfected at day -3 and again at day 0 (starting reprogramming by adding DOX) with siRNA for cMyc, lMyc, nMyc or control (Stealth siRNA- mix of 3 as indicated in the table below) with RNAiMAX (Invitrogen). For molecular analysis, cells were collected at day 3 and day 7 or day 8 as indicated.

### Generation of triple Tet1,2,3<sup>flox/flox</sup> mice and cell lines

Tet2<sup>flox/flox</sup> mice were obtained from Jackson Laboratories (Stock number 017573). Tet1<sup>flox/flox</sup> mice were generated by using conditional knockout targeting vector against Exon 4 in V6.5 ESC. After removal of Neomycin selection cassettes by Flippase in correctly targeted ESCs (validated both by Southern Blot and PCR analysis), chimeric blastocyst injections followed by successful germline transmission allowed us to establish Tet1<sup>flox/flox</sup> mouse colony. Tet3<sup>flox/flox</sup> mice were generated by gene targeting of the endogenous Exon 7 (contains Fe(ii) catalytic domain) Tet3 locus. After removal of Neomycin selection cassettes by Flippase in correctly targeted ESCs (validated both by Southern Blot and PCR analysis), chimeric blastocyst injections followed by successful germline transmission allowed us to establish Tet3<sup>flox/flox</sup> mouse colony. Triple floxed homozygous mice were generated by interbreeding, after which Tet1<sup>flox/flox</sup> Tet2<sup>flox/flox</sup> Tet3<sup>flox/flox</sup> mouse strain was obtained. Genotyping primers: Tet1\_gen1\_F: AGGAGTGTTCAGGTTCAAGGCCATC; Tet1\_gen1\_R:TCCCTGACAGCAGCCACACTTG; Tet2\_lox\_F: AAGAATTGCTACAGGCCTGC; Tet2\_lox\_R: TTCTTTAGCCCTTGCTGAGC; Tet3\_lox\_f: agttcctgacgttgagagttgg; Tet3\_lox\_r: ggaactcaagctcctcagaggaagc. The Tet1 floxed allele gives a band of 500bp, compared to the 450bp WT. The Tet2 flox allele gives a band of 427bp, compared to the 249bp WT. The Tet3 floxed allele gives a band of 300bp, compared to the 200bp WT. MEFs, ESCs and iPSCs were derived from triple Tet1/2/3<sup>flox/flox</sup> mice and were used as indicated in the figures. Deleting Gatad2a in Tet1/2/3<sup>flox/flox</sup> iPSCs was done with CRISPR/Cas9 as indicated in methods above.

### RT-PCR analysis

Total RNA was isolated using Trizol (ThermoFisher). 1 µg of DNase-I-treated RNA was reverse transcribed using a First Strand Synthesis kit (Invitrogen) and ultimately re-suspended in 100 µl of water. Quantitative PCR analysis was performed in triplicate using 1/50 of the reverse transcription reaction on Vii7 platform (Applied Biosystems). Error bars indicate standard deviation of triplicate measurements for each measurement.

## AP Staining

Alkaline phosphatase (AP) staining was performed with AP kit (Millipore SCR004) according to manufacturer's instructions.

## Imaging, quantifications, and statistical analysis

Images were acquired with D1 inverted microscope (Carl Zeiss, Germany) equipped with DP73 camera (Olympus, Japan) or with Zeiss LSM 700 inverted confocal microscope (Carl Zeiss, Germany) equipped with 405nm, 488nm, 555nm and 635 solid state lasers, using a 20x Plan-Apochromat objective (NA 0.8). All images were acquired in sequential mode. For comparative analysis, all parameters during image acquisition were kept constant throughout each experiment. Images were processed with Zen blue 2011 software (Carl Zeiss, Germany), and Adobe Photoshop.

## ChIP-seq library preparation

Cells were crosslinked in formaldehyde (1% final concentration, 10 min at room temperature), and then quenched with glycine (5 min at room temperature). Fixed cells were lysed in 50 mM HEPES KOH pH 7.5, 140 mM NaCl, 1 mM EDTA, 10% glycerol, 0.5% NP-40 alternative, 0.25% Triton supplemented with protease inhibitor at 4 °C (Roche, 04693159001), centrifuged at 950g for 10 min and re-suspended in 0.2% SDS, 10 mM EDTA, 140 mM NaCl and 10 mM Tris-HCl. Cells were then fragmented with a Branson Sonifier (model S-450D) at -4 °C to size ranges between 200 and 800 bp and precipitated by centrifugation. Antibody was pre-bound by incubating with Protein-G Dynabeads (Invitrogen 100-07D) in blocking buffer (PBS supplemented with 0.5% TWEEN and 0.5% BSA) for 1 h at room temperature. Washed beads were added to the chromatin lysate for an incubation periods of either 6 or 18 hours. Samples were washed five times with RIPA buffer, twice with RIPA buffer supplemented with 500 mM NaCl, twice with LiCl buffer (10 mM TE, 250mM LiCl, 0.5% NP-40, 0.5% DOC), once with TE (10mM Tris-HCl pH 8.0, 1mM EDTA), and then eluted in 0.5% SDS, 300 mM NaCl, 5 mM EDTA, 10 mM Tris HCl pH 8.0. Eluate was incubated treated sequentially with RNaseA (Roche, 11119915001) for 30 min and proteinase K (NEB, P8102S) for 2 h in 65 °C for 8 h, and then. DNA was purified with The Agencourt AMPure XP system (Beckman Coulter Genomics, A63881). Libraries of cross-reversed ChIP DNA samples were prepared according to a modified version of the Illumina Genomic DNA protocol. All chromatin immunoprecipitation data are available at the National Center for Biotechnology Information Gene Expression Omnibus database under the series accession GEO no. [GSE102518](https://www.ncbi.nlm.nih.gov/geo/query/acc.cgi?acc=GSE102518). Samples were run with various protocols and machines (Table S1). Please note that while it seems that Klf4 is starting to significantly bind enhancers only on day 2, we note that this is actually a result of the specific Klf4 antibody used for ChIP-seq, that is known to have better affinity for endogenous form of mouse Klf4 which becomes highly upregulated later in reprogramming, than the exogenous transgene derived human KLF4 version that is induced from early stage upon DOX addition.

### PolyA-RNA-seq library preparation

Total RNA was isolated from indicated cell lines, RNA was extracted from Trizol pellets by Directzol RNA MiniPrep kit (Zymo) and utilized for RNA-Seq by TruSeq RNA Sample Preparation Kit v2 (Illumina) according to manufacturer's instruction. See Table S1 for details of protocol and sequencing machine used.

### Small RNA-seq library preparation

1 µg of total RNA from each sample was processed using the TruSeq small RNA sample preparation kit (RS-200-0012 Illumina) followed by 12 cycles of PCR amplification. Libraries were evaluated by Qubit and TapeStation. For purification of the small RNA fragments, they were size selected using Blupippne machine (Sage Science) with 3% gel cassette followed by clean-up with minielute PCR purification kit (Qiagen). The libraries were constructed with different barcodes to allow multiplexing of 11 samples. See Table S1 for details of protocol and sequencing machine used.

### ATAC-seq library preparation

Cells were trypsinized and counted, 50,000 cells were centrifuged at 500g for 3 min, followed by a wash using 50 µl of cold PBS and centrifugation at 500g for 3 min. Cells were lysed using cold lysis buffer (10 mM Tris-HCl, pH 7.4, 10 mM NaCl, 3 mM MgCl<sub>2</sub> and 0.1% IGEPAL CA-630). Immediately after lysis, nuclei were spun at 500g for 10 min using a refrigerated centrifuge. Next, the pellet was resuspended in the transposase reaction mix (25 µl 2× TD buffer, 2.5 µl transposase (Illumina) and 22.5 µl nuclease-free water). The transposition reaction was carried out for 30 min at 37 °C and immediately put on ice. Directly afterwards, the sample was purified using a Qiagen MinElute kit. Following purification, the library fragments were amplified using custom Nextera PCR primers 1 and 2 for a total of 12 cycles. Following PCR amplification, the libraries were purified using a Qiagen MinElute Kit and sequenced as indicated in Table S1.

### Whole-Genome Bisulfite Sequencing (WGBS) library preparation

DNA was isolated from snap-frozen cells using the Quick-gDNA mini prep kit (Zymo). DNA was then converted by bisulfite using the EZ DNA Methylation-Gold kit (Zymo). Sequencing libraries were created using the EpiGnome Methyl-Seq (Epicentre) and sequenced as indicated in Table S1

### Reduced-Representation Bisulfite (RRBS) library preparation

RRBS libraries were generated as described previously with slight modifications<sup>40</sup>. Briefly, DNA was isolated from snap-frozen cell pellets using the Quick-gDNA mini prep kit (Zymo). Isolated DNA was then subjected to MspI digestion (NEB), followed by end repair using T4 PNK/T4 DNA polymerase mix (NEB), A-tailing using Klenow fragment (3'5' exo-) (NEB), size selection for fragments shorter than 500 bp using SPRI beads (Beckman Coulter) and ligation into a plasmid using quick T4 DNA ligase (NEB). Plasmids were treated with sodium bisulphite using the EZ DNA Methylation-Gold kit (Zymo) and the product was PCR amplified using GoTaq Hot Start DNA polymerase (Promega). The PCR products were A-tailed using Klenow fragment, ligated to indexed Illumina adapters using



quick T4 DNA ligase and PCR amplified using GoTaq DNA polymerase. The libraries were then size-selected to 200–500 bp by extended gel electrophoresis using NuSieve 3:1 agarose (Lonza) and gel extraction (Qiagen). See Table S1 for sequencing protocol used.

## Quantification and Statistical Analysis

### ChIP-seq analysis

**Alignment and peak detection**—We used bowtie2 software to align reads to mouse mm10 reference genome (UCSC, December 2011), with default parameters. We identified enriched intervals of all measured proteins using MACS version 1.4.2-1. We used sequencing of whole-cell extract as control to define a background model. Duplicate reads aligned to the exact same location are excluded by MACS default configuration.

**TSS, TES and Enhancer definition**—Transcription start sites (TSS) and transcription end sites (TES) were taken from mm10 assembly (UCSC, December 2011). Promoters/TES intervals were defined as 1000bp around each TSS/TES, and enhancers were defined as 300bp around enhancer detection summit point (see enhancer identification below).

**Chromatin modification profile estimation in TSS, TES and in enhancers**—Chromatin modification coverage in the genomic intervals was calculated using in-house script. Shortly, the genomic interval is divided to 50bp size bins, and the coverage in each bin is estimated. Each bin is then converted to z-score by normalizing by the mean and standard deviation of the sample noise ( $X^*_j = (X_j - \mu_{\text{noise}}) / \sigma_{\text{noise}}$ ). Noise parameters were estimated for each sample from  $6 \times 10^7$  random bp across the genome. Finally, the 3<sup>rd</sup> highest bin z-score of each interval is set to represent the coverage of that interval.

**Transcription factor binding in promoter and enhancer**—Promoter or enhancer was defined as bound by a TF if it overlapped a binding peak of the TF, as detected by MACS. Of note, 94.3% of the identified peaks of OSK overlap with either promoter or enhancer.

**Transcription factor binding taken from previously published data (Chronis et al. Cell 2017)**—OSKM/Runx1 Binding data were downloaded from NCBI GEO GSE90893, and were analyzed using the same pipeline as described above.

### RNA-seq analysis

**Read Alignment for PolyA-RNA-seq**—Tophat software version 2.0.10 was used to align reads to mouse mm10 reference genome (UCSC, December 2011). FPKM values were calculated over all genes in mm10 assembly GTF (UCSC, December 2011), using cufflinks (version 2.2.1). Genes annotated as protein coding, pseudogene or lncRNA (n=24,439) were selected for further analysis.

**Read Alignment for Small RNA-seq**—Bowtie software version 2 was used to align reads to mouse mm10 reference genome (UCSC, December 2011). FPKM values were calculated over all genes in mm10 assembly GTF (UCSC, December 2011), using cufflinks (version 2.2.1) (Trapnell et al., 2010).

Genes annotated as rRNA, miRNA, snoRNA were selected for further analysis.

Subsequently, PolyA and small RNA-seq FPKM were combined and processed together.

**Active and Differential genes**—Gene was defined to be active in samples where FPKM is above 0.5 of the gene max value. Differential genes were defined by  $(FC > 4)$  &  $(\text{maximum value} > 1)$ . Subsequent filtering was done to reject oscillatory or non-continuous time series by comparing the sum of derivatives to the total span. Specifically, the filtering scheme is  $\sum_{j>1} (R^i_j - R^i_{j-1}) / (\max_j(R^i_j) - \min_j(R^i_j)) < 2.5$ , where  $j$  is the sample index, and  $i$  is the gene index.

**Expression HeatMap**—Gene sorting in expression heat-maps (Fig. 1G) was done according to the average position of gene active samples, i.e. calculating the average of sample indexes ( $j$ ) where the gene is active. **Unit normalized FPKM** was calculated using the following formula  $R^i_{j*} = R^i_j / [\max_j(R^i_j) + 1]$  where  $j$  is the sample index,  $i$  is the gene index and  $FPKM=1$  is the transcription noise threshold, and  $\max_j(R^i_j)$  is the maximal level in each dataset. This normalization scheme allowed easy comparison of gene temporal pattern with normalized dynamic range.

**Correlations**—All correlation tests were done using Spearman correlation.

**PCA** PCA analysis (Fig. 1H) was carried out over all differential genes in unit normalization by Matlab (version R2011b) princomp command.

### Analysis and integration of previously published datasets

C/EBPa+OSKM B cell reprogramming RNA-seq data was downloaded from NCBI GEO database GSE96611, and was analyzed using the same pipeline as described above.

### Extended Differential lncRNA analysis

lncRNA dataset was annotated using PLAR. FPKM values were calculated for all lncRNAs in PLAR mm9 dataset using cuffdiff (version 2.2.1) (Trapnell et al., 2010). lncRNA coordinates were then converted to mm10 using liftOver utility. Differential lncRNAs were defined by  $(FC > 4)$  &  $(\text{maximum value} > 1)$ . Subsequent filtering removed lncRNAs that were suspected to be expressed due to B1/B2-repeats by removing all sequence reads overlapping B1 or B2 repeats, resulting in 560 differential lncRNAs, out of them 221 differential lncRNA not previously annotated by Ensembl (Table S2). Hierarchical clustering was performed over all differential lncRNAs with Spearman correlation metric and average linkage, further separating the differential lncRNAs to up, down regulated and intermediate induced lncRNAs (Table S3).

RNA-seq data are available at the National Center for Biotechnology Information Gene Expression Omnibus database under the series accession GEO no. [GSE102518](https://www.ncbi.nlm.nih.gov/geo/query/acc.cgi?acc=GSE102518).

### Phylogenetic analysis

Conservation scores of CAPGs and ESPGs were extracted from PhyloGene database (Sadreyev et al., 2015) <http://genetics.mgh.harvard.edu/phylogene/>.

## Functional Enrichment

Active genes at each sample (day) are tested for enrichment of functional gene sets taken from Gene Ontology (GO, <http://www.geneontology.org>), using Fisher exact test. Gene is defined to be active in samples where FPKM is above 0.5 of the gene max value. All enrichment values for each day were FDR corrected using Benjamini and Hochberg method. GO annotations were filtered to include only annotations with FDR-corrected  $p\text{-val} < 0.01$  in at least two samples, annotations are sorted according to average position of enrichment pattern.

## Protein-DNA binding enrichment analysis

Active genes at each sample (day) are tested for enrichment (fisher exact test) to previously published protein-DNA binding ChIP-seq obtained from the Compendium, hmChip and BindDB databases. Gene is defined to be active in samples where RPKM is above 0.5 of the gene max value. All enrichment values for each day were passed through FDR test, using the Benjamini and Hochberg method. Subsequently, TF annotations per day were filtered to include only annotations with FDR-corrected  $P\text{val} < 10^{-30}$  in at least one sample. Further filtering the predicted TF to include only TF that are also differentially expressed during reprogramming according to our collected RNA-seq. The resulting predicted TF's and their connectivity map from Compendium and hmChip are then merged where any connection exists in one of the databases also appears in the resulted connectivity matrix.

## ATAC-seq analysis

Reads were aligned to mm10 mouse genome using Bowtie2 with the parameter `-X2000` (allowing fragments up to 2 kb to align). Duplicated aligned reads were removed using Picard MarkDuplicates tool with the command `REMOVE_DUPLICATES=true`. To identify chromatin accessibility signal we considered only short reads ( $\approx 100\text{bp}$ ) that correspond to nucleosome free region. C/EBPa+OSKM B cell reprogramming ATAC-seq data was downloaded from NCBI GEO database GSE96611, and was analyzed using the same pipeline as described above.

## Identifying accessible chromatin regions

To detect and separate accessible loci in each sample, we used MACS version 1.4.2-1 with `--call-subpeaks` flag (PeakSplitter version 1.0). Next, summits in previously annotated spurious regions were filtered out using a custom blacklist targeted at mitochondrial homologues. To develop this blacklist, we generated 10,000,000 synthetic 34mer reads derived from the mitochondrial genome. After mapping and peak calling of these synthetic reads we found 28 high-signal peaks for the mm10 genome. For all subsequent analysis, we discarded peaks falling within these regions.

## Enhancer Identification

Each ATAC-seq peak in each sample was represented by a 300bp region around the summit center. H3K27ac peaks were detected in a similar manner, using MACS version 1.4.2-1, and merged for all time points using bedtools merge command. All ATAC peaks were filtered to include only peaks which co-localized with the merged H3K27ac peaks, meaning only

ATAC peaks that have H3K27ac mark on at least one of the time points were passed to further processing. Finally, the peaks from all samples were unified and merged (using bedtools unionbedg and merge commands), further filtered to reject peaks that co-localized with promoter or exon regions based on mm10 assembly (UCSC, December 2011). Finally we were left with 93,137 genomic intervals which we annotated as active enhancers, of which 78% of overlap with H3K4me1 modification, and 69.9% are bound by at least one of the transcription factors mapped (RNA PolII/O/S/K/M), and 54% are bound by at least one of O/S/K. MEF-enhancers significantly overlap with ENCODE Spleen and Heart enhancers (p-value<1e-13, Enrichment fold-change > 1.4), and Day7 & Day8 enhancers significantly overlap with ENCODE mESC enhancers (p-value<3.2e-11, Enrichment fold-change > 1.3). All enhancers were then annotated by their most proximal gene using annotatePeaks function (homer/4.7 package). Enhancers were considered as differential if both their ATAC-seq and H3K27ac signals show significant change during reprogramming (min zscore<0.5, max zscore>1.5, for both chromatin marks). ATAC-seq data are deposited under GEO no. [GSE102518](https://www.ncbi.nlm.nih.gov/geo/query/acc.cgi?acc=GSE102518).

### Generating ATAC-seq normalized profiles in TSS and in enhancers

ATAC-seq profiles were calculated using in-house script over all genomic intervals defined for TSS and enhancers. Shortly, the genomic interval is divided to 50bp size bins, and the coverage in each bin is estimated. Each bin is then converted to z-score by normalizing each position by the mean and standard deviation of the sample noise ( $\hat{X}_j = (X_j - \mu_{\text{noise}}) / \sigma_{\text{noise}}$ ). Noise parameters were estimated for each sample from  $6 \times 10^7$  random bp across the genome. Finally, the 3<sup>rd</sup> highest bin z-score of each interval is set to represent the coverage of that interval.

## Methylation Analysis of WGBS and RRBS

### Alignment of RRBS data

The sequencing reads were aligned to the mouse mm10 reference genome (UCSC, December 2011), using Bismark aligner (Krueger and Andrews, 2011) (parameters -n 1 -l 20). Mapping was done independently for the two ends of each pair. Read pairs that mapped uniquely to two different fragments were discarded. In cases where one read uniquely mapped on a restriction site but its pair could not be mapped uniquely or could not be mapped at all, we attempted to re-align the entire read pair to the fragment. Read pairs showing more than one unconverted non-CpG cytosine, which occur at very low frequency were filtered out.

### Alignment of WGBS data

The sequencing reads were aligned to the mouse mm10 reference genome (UCSC, December 2011), using a proprietary script based on Bowtie2. In cases where the two reads were not aligned in a concordant manner, the reads were discarded.

## Methylation estimation

Methylation levels of CpGs calculated by RRBS and WGBS were unified. Mean methylation was calculated for each CpG that was covered by at least 5 distinct reads (X5). Average methylation level in various genomic intervals was calculated by taking the average over all covered X5 covered CpG sites in that interval. Please note that in both systems higher global DNA methylation levels were observed in iPSC that were cultured over prolonged time in 2i/LIF conditions, compared to newly generated iPSCs on day 8 possibly because OSKM transgene can boost hypomethylation independent of 2i.

## Correlation of chromatin modifications

Correlation between chromatin modification to gene expression and to accessibility signal were estimated using Spearman correlation (Figure 4a, 5a, S2C-D). Promoters or enhancers with z-score above zero were included in the analysis, resulting in different number of promoter or enhancers for each chromatin marks (which are indicated in the figures).

## Cross-correlation of chromatin modifications

Cross correlation method<sup>50,51</sup> measures the overlap between two signals, while shifting the signals in their x-axis (convolution). In our case, the x-axis is time. Cross correlation score was calculated using Matlab R2013b `xcorr` command. The offset showing the highest `xcorr` coefficient was defined as the optimal offset between the two signals. Cross-correlation was calculated in three systems: (i) Between chromatin modifications in promoters and gene expression pattern of ESPGs (Fig. 5C). (ii) Between chromatin modifications and accessibility signal in differential enhancers (Fig. 5D). (iii) Between chromatin modifications in promoters and enhancers that are associated with these promoters, and gene expression (Fig. S7A).

In all these cases promoters/enhancers were included only if the modification z-score was changing ( $\max - \min > 0.5$ ), resulting in different number of promoters/enhancers as indicated in the graphs. Please note that we could not present cross-correlation with OSKM binding, because the method requires quantitative information (z-score), and we used OSKM binding only as binary data (MACS binding peaks).

## Combinatorial analysis for histone marks localization

To quantify all possible combinations of epigenetic modifications (Fig. 5B,5E, S5F), we transformed our epigenetic data to a binary code in each genomic region (promoter/enhancer). Each epigenetic mark in promoter or enhancer was considered high (value=1) if its z-score was above 1.5. For each sample, the percentage of each combination is presented. Combinations which are less than 3% of the total combinations in every sample are presented as “other” (gray color). Up-regulated ESPGs were selected if their fold-change was as follows:  $\text{mean}(\text{Day8,iPS})/\text{mean}(\text{MEF,Day1}) > 4$ . Down-regulated ESPGs were selected if their fold change was as follows:  $\text{mean}(\text{MEF,Day1})/\text{mean}(\text{Day8,iPS}) > 4$ .

## Motif analysis

Enriched binding motifs were searched in various genomic intervals using findMotifsGenome function from homer software package version 4.7, using the software default parameters.

## Motif analysis in open vs. closed binding targets

In order to find binding motifs in open vs. closed binding targets (Fig. 2G) we followed the analysis outline presented by Soufi et al (Soufi et al., 2015): We considered binding peaks of O/S/K/M in Day1, identified by MACS as explained. We calculated nucleosome occupancy in a 200bp window in the summit of the peak, and in two 100bp flanking regions on the two sides of the central window. Nucleosome occupancy was estimated from ATAC-seq data, measured in Day1, using nucleoatac occ software. Top 2000 binding sites with highest center/flanking ratio were selected as closed sites (as long as ratio >1), and bottom 2000 sites were selected as open sites (as long as ratio <1). Next, motif search and annotation was done as in (Soufi et al., 2015), using DREME, Centrimo and TOMTOM software, of MEME suite.

## Box plot analysis

Box-plots show 25-th and 75-th percentile of the represented distribution values, with median marked by the mid-line. The whiskers extend to the most extreme data point which is no more than 1.5 times the interquartile range from the box, and outliers are not presented.

## Translation Analysis

### Coding sequences

The coding sequences of *M. musculus* were downloaded from the Consensus CDS (CCDS) project (<ftp://ftp.ncbi.nlm.nih.gov/pub/CCDS/>).

### tRNA gene copy numbers

The tRNA gene copy numbers of *M. musculus* were downloaded from the Genomic tRNA Database (<http://lowelab.ucsc.edu/GtRNAdb/>).

### Estimating translational efficiency by chromatin modification signature in the vicinity of tRNAs

We estimated translation efficiency of genes using the “tRNA activation index” (tACI) which was introduced previously by (Gingold et al., 2014). This measure is calculated similarly to the tRNA Adaptation Index (tAI) measure of translation efficiency (dos Reis et al., 2004), with one change—tRNA availabilities are determined based on chromatin modification in the vicinity of the tRNA genes rather than by gene copy numbers. Specifically, we set the activation score of each individual tRNA gene to be the maximal read per megabase (RPM) value of the activation-associated modification H3K4me3 across a region spanning the 500 nucleotides upstream to the first nucleotide of the mature tRNA. Individual tRNA genes, for which no signal enrichment was found, were classified as “not



activated.” Next, we defined the activation score of each tRNA type (anticodon) by the sum of the activation scores of its gene copies. Then, we determined the translation efficiency of each of the 61 codon types by the extent of activation of the tRNAs that serve in translating it, incorporating both the fully matched tRNA as well as tRNAs that contribute to translation through wobble rules. Formally, the translation efficiency score for the  $i$ -th codon is

$$W_i = \sum_{j=1}^{n_i} (1 - s_{ij}) tCME_{ij}$$

where  $n$  is the number of types of tRNA isoacceptors that recognize the  $i$ -th codon,  $tCME_{ij}$  denotes the sum of the chromatin modification scores of the activated copies of the  $j$ -th tRNA that recognizes the  $i$ -th codon, and  $S_{ij}$  corresponds to the wobble interaction, or selective constraint on the efficiency of the pairing between codon  $i$  and anticodon  $j$ , as was determined and implemented for the original tAI measure. As done in the original tAI formalism by the scores of the 61 codons are further divided by the maximal score (yielding  $w_i$  as the normalized scores for each codon type), and finally, the tACI value of a gene with  $L$  codons is then calculated as the geometric mean of the  $w_i$ 's of its codons

$$tACI(g) = L \sqrt[L]{\prod_{c=1}^L w_c}$$

## Supplementary Material

Refer to Web version on PubMed Central for supplementary material.

## Acknowledgements

J.H.H is supported by a gift from Ilana and Pascal Mantoux, and grants from: European Research Council, FAMRI, Israel Science Foundation (ISF-ICORE, NFSC, Morasha (also to N.N.)), Kamin-Yeda, Minerva, ICRF, BSF, Human Frontiers Science Program (HFSP), the Benozio Endowment fund, NYSCF, Kimmel Innovator Research Award, the Helen and Martin Kimmel Institute for Stem Cell Research. J.H.H. is a NYSCF–Robertson Investigator.

## Data Availability

All RNA-seq, ATAC-seq, ChIP-seq and methylation data are available to download from NCBI GEO, under super-series GSE102518.

## References

- Carey BW, Markoulaki S, Beard C, Hanna J, Jaenisch R. Single-gene transgenic mouse strains for reprogramming adult somatic cells. *Nat Methods*. 2010; 7:56–59. [PubMed: 20010831]
- Chronis C, Fiziev P, Papp B, Butz S, Bonora G, Sabri S, Ernst J, Plath K. Cooperative Binding of Transcription Factors Orchestrates Reprogramming. *Cell*. 2017; 168:442–459. [PubMed: 28111071]
- Gingold H, Tehler D, Christoffersen NR, Nielsen MM, Asmar F, Kooistra SM, Christophersen NS, Christensen LL, Borre M, Sørensen KD, et al. A Dual Program for Translation Regulation in Cellular Proliferation and Differentiation. *Cell*. 2014; 158:1–22.

- Hussein SMI, Puri MC, Tonge PD, Benevento M, Corso AJ, Clancy JL, Mosbergen R, Li M, Lee D-S, Cloonan N, et al. Genome-wide characterization of the routes to pluripotency. *Nature*. 2014; 516:198–206. [PubMed: 25503233]
- Kiviet DJ, Nghe P, Walker N, Boulineau S, Sunderlikova V, Tans SJ. Stochasticity of metabolism and growth at the single-cell level. *Nature*. 2014; 5124:376–9.
- Lee DS, Shin JY, Tonge PD, Puri MC, Lee S, Park H, Lee WC, Hussein SMI, Bleazard T, Yun JY, et al. An epigenomic roadmap to induced pluripotency reveals DNA methylation as a reprogramming modulator. *Nat Commun*. 2014; 5
- Li D, Liu J, Yang X, Zhou C, Guo J, Wu C, Qin Y, Guo L, He J, Yu S, et al. Chromatin Accessibility Dynamics during iPSC Reprogramming. *Cell Stem Cell*. 2017; 21:819–833. [PubMed: 29220666]
- Mor N, Rais Y, Sheban D, Peles S, Aguilera-Castrejon A, Zviran A, Elinger D, Viukov S, Geula S, Krupalnik V, et al. Neutralizing Gatad2a-Chd4-Mbd3/NuRD Complex Facilitates Deterministic Induction of Naive Pluripotency. *Cell Stem Cell*. 2018; 23:412–425. [PubMed: 30122475]
- Nakagawa M, Koyanagi M, Tanabe K, Takahashi K, Ichisaka T, Aoi T, Okita K, Mochiduki Y, Takizawa N, Yamanaka S. Generation of induced pluripotent stem cells without Myc from mouse and human fibroblasts. *Nat Biotechnol*. 2008; 26:101–106. [PubMed: 18059259]
- Polo JM, Anderssen E, Walsh RM, Schwarz BA, Nefzger CM, Lim SM, Borkent M, Apostolou E, Alaei S, Cloutier J, et al. A molecular roadmap of reprogramming somatic cells into iPSC cells. *Cell*. 2012; 151:1617–1632. [PubMed: 23260147]
- Rahl PB, Lin CY, Seila AC, Flynn RA, McCuine S, Burge CB, Sharp PA, Young RA. c-Myc regulates transcriptional pause release. *Cell*. 2010; 141:432–445. [PubMed: 20434984]
- Rais Y, Zviran A, Geula S, Gafni O, Chomsky E, Viukov S, Mansour AA, Caspi I, Krupalnik V, Zerbib M, et al. Deterministic direct reprogramming of somatic cells to pluripotency. *Nature*. 2013; 502:65–70. [PubMed: 24048479]
- Scognamiglio R, Cabezas-Wallscheid N, Thier MC, Altamura S, Reyes A, Prendergast ÁM, Baumgärtner D, Carnevalli LS, Atzberger A, Haas S, et al. Myc Depletion Induces a Pluripotent Dormant State Mimicking Diapause. *Cell*. 2016; 164:668–680. [PubMed: 26871632]
- Soufi A, Garcia MF, Jaroszewicz A, Osman N, Pellegrini M, Zaret KS. Pioneer transcription factors target partial DNA motifs on nucleosomes to initiate reprogramming. *Cell*. 2015; 161:555–568. [PubMed: 25892221]
- Di Stefano B, Sardina JL, Van Oevelen C, Collombet S, Kallin EM, Vicent GP, Lu J, Thieffry D, Beato M, Graf T. C/EBPα poises B cells for rapid reprogramming into induced pluripotent stem cells. *Nature*. 2014; 506:235–9. [PubMed: 24336202]
- Stelzer Y, Shivalila CS, Soldner F, Markoulaki S, Jaenisch R. Tracing Dynamic Changes of DNA Methylation at Single-Cell Resolution. *Cell*. 2015; 163:218–229. [PubMed: 26406378]
- Takahashi K, Yamanaka S. Induction of Pluripotent Stem Cells from Mouse Embryonic and Adult Fibroblast Cultures by Defined Factors. *Cell*. 2006; 126:663–676. [PubMed: 16904174]

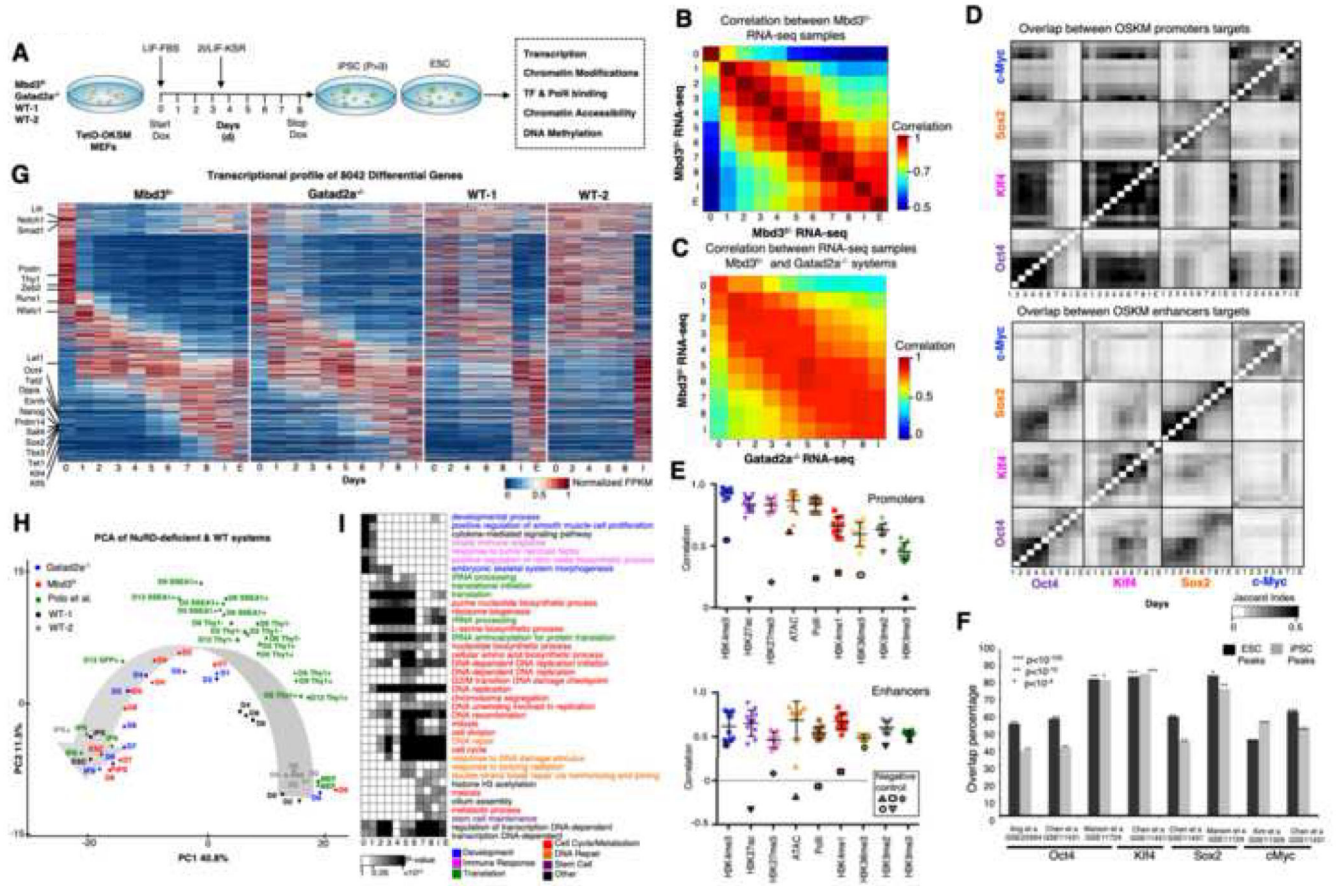


**Fig. 1. Continuous and coordinated progression of conducive reprogramming in two independent NuRD-deficient systems.**

**A.** Experimental scheme. **B.** Spearman correlation between expression profiles of Mbd3<sup>flx</sup>-system Calculated over all differential genes (n=8,042), showing an average correlation of R=0.93 between consecutive samples. **C.** As in **B**, but between Mbd3<sup>flx</sup> and Gatad2a<sup>-/-</sup> systems. **D.** Overlap between targets of OSKM in promoters and enhancers. Pixel shade indicates Jaccard Index. **E.** Correlation between consecutive samples in Mbd3<sup>flx</sup> system (MEF-day1, day1-day2, day2..day8-iPS), measured over all ESPGs promoters (promoters with differential chromatin pattern, n=3,593, top), or all differential enhancers (n=40,174, bottom), for each chromatin mark. Negative controls were calculated between MEF and IPS, are marked with solid border. **F.** Overlap between binding targets of Oct4, Sox2, Klf4 or Myc, and previously published binding data of the same factors, calculated in ES and iPSC samples. Percentage out of our measured binding targets is presented, along Fisher exact test p-values. **G.** Global transcriptional pattern of 8,042 differential genes (FC>4 & maximal FPKM value>1), sorted by their temporal pattern in Mbd3<sup>flx</sup>-system (the same gene order was applied for the other reprogramming systems). Heatmap represents unit-transformation of FPKM values. **H.** PCA analysis of all samples, alongside samples from previous publications (Polo et al., 2012). PCA was calculated on the same set of genes and normalization as in **G**. **I.** GO categories enriched among the genes that are active in each day. Gene is defined to be active in samples where RPKM is above 0.5 of the gene max

value. P-values were calculated with Fisher exact test, and FDR corrected. Categories with corrected p-value<0.01 in at least two-time points are presented. Gray Shades represent FDR corrected p-values



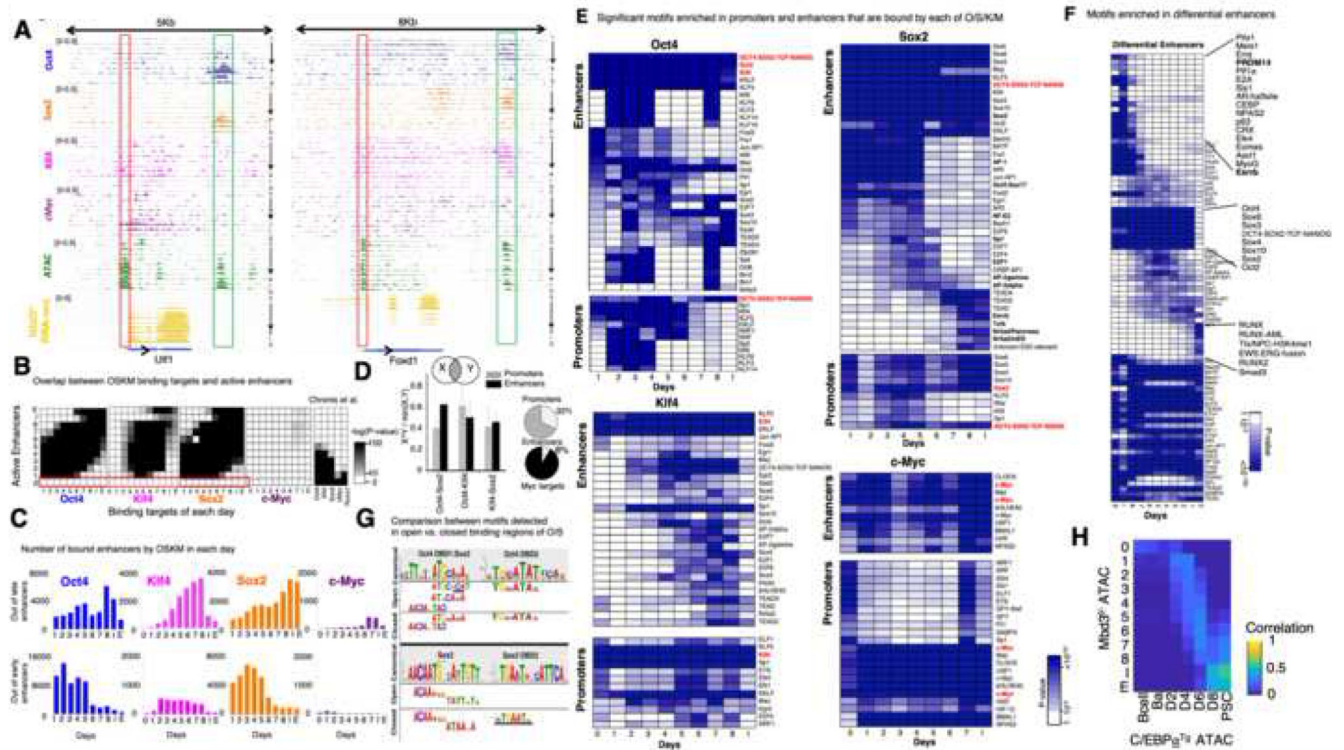


**Fig. 2. Stage-specific binding preference and collaboration of OSKM.**

**A.** ChIP-seq landscape of two examples. Promoters are marked in red, enhancers are marked in green. Signals are normalized to sample size (RPM). **B.** Overlap between binding of OSKM and active enhancers, in each day of reprogramming. Enhancer is defined as active in a specific day if its ATAC-seq z-score is above 1.5 STD in that day. Gray shades indicate Fisher exact test p-value for overlap between compared samples. Note that OSKM do not bind the enhancers that are active in MEF (D0, marked in red); these enhancers are not significantly bound by OSKM at any day during reprogramming. **C.** Number of enhancers bound by each of OSKM factors in each day of reprogramming. Upper row: out of enhancers that are bound by the factor in late stages (day8, iPS, ESC). Bottom row: out of enhancers that are bound by the factor in early stages (day1-day3). **D.** Probability to observe co-localized binding of transcription factors in promoters (gray) and enhancers (black). Calculated in days 1,8 and iPS (Error bars indicate S.E.M). Right – Myc binds 32% of promoters, and 8% of active enhancers. **E.** Significant motifs enriched in promoters and enhancers that are bound by each of Oct4, Sox2, Klf4 and c-Myc at different days of reprogramming, as detected by Homer/4.7 software. P-values, indicated by color shade, were reported by Homer, and are FDR corrected. Motifs which are significantly enriched (corrected  $p < 10^{-30}$ ) in at least one time point are presented. **F. a.** Motifs enriched in differential enhancers that are active in each day of reprogramming (ATAC-seq z-score  $> 1.5$ ). P-values, indicated by color shade, were reported by Homer, and are FDR corrected. Motifs which are significantly enriched (corrected  $p < 10^{-50}$ ) in at least one-time point are presented. **G.** Motifs found in “closed” vs. “open” binding targets of the indicated transcription factor. Accessibility of targets was calculated based on ATAC-seq. Motifs

found in OSK binding targets calculated in  $Mbd3^{f/-}$  day1. Motifs that are different between open and closed binding targets are marked in black line. Complementary motifs to canonical motif appear in reverse order. **H.** Spearman correlation between ATAC-seq profiles of the two efficient reprogramming systems:  $Mbd3^{f/-}$  MEF and  $C/EBP\alpha^{Tg}$  B cell systems calculated over 40,174 differential enhancers.



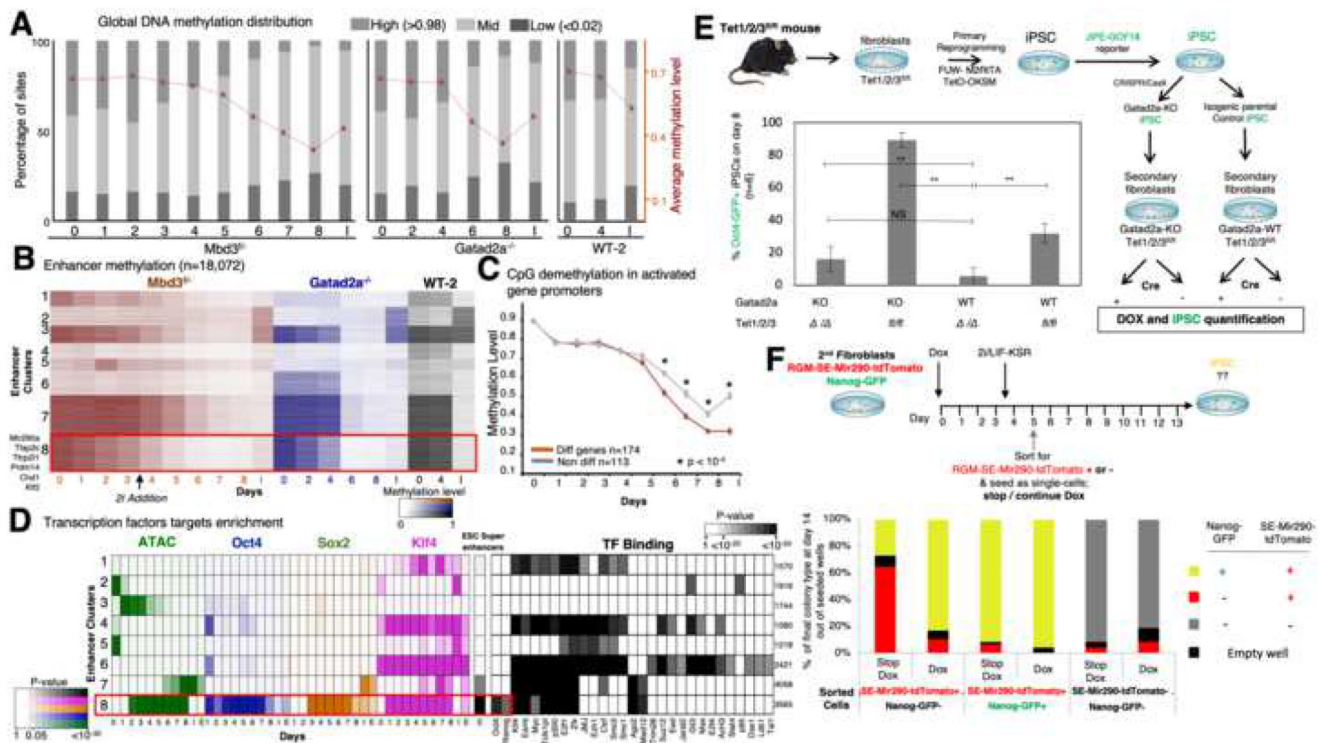


**Fig. 3. Rapid DNA-demethylation of naïve ESC super-enhancers during conducive iPSC reprogramming.**

**A.** Distribution of low (<0.02), mid (0.02-0.98) and high (>0.98) methylated CpG sites, along reprogramming. Average and SEM are indicated in red plot. **B.** Methylation level measured in covered enhancers (n=18,072), in *Mbd3<sup>fl/fl</sup>*, *Gatad2a<sup>-/-</sup>* and WT-2 systems. Enhancers are clustered into eight clusters using k-means. Cluster 8 consists of enhancers that undergo fast demethylation, compared to clusters 3 and 7. **C.** Average methylation measured in promoters of genes that were highly methylated (>80%) in day0. Genes that change their expression level (red) are compared to genes that do not change their expression level (gray). Wilcoxon p-value indicates places where methylation of differential genes is significantly lower than methylation of non-differential genes. **D. Left:** Enrichment of enhancer clusters, as shown in panel B, for OSK binding, DNA accessibility, and super enhancers, showing that cluster 8 is highly enriched for OSK binding and overlaps with super enhancers. Color shades represent FDR corrected enrichment p-value. **Right:** Enrichment of the same enhancer clusters to transcription factor binding, taken from hmChIP database. Cluster size is indicated on the right. **E.** Experimental scheme summary. Reprogramming efficiency was measured by Oct4-GFP+ cells percentage in *Tet1/2/3* null( ) and *Tet1/2/3<sup>fl/fl</sup>* with and without *Gatad2a* expression, after 8 days. \*\*p<0.01, \*\*\*p<0.001 (Student's t-test), n=6, error bars indicate SD. **F.** Secondary MEF harboring *Mir290*-RGM and *Nanog* GFP-reporter were sorted after reprogramming to 3 different populations: RGM-*SE-Mir290*-tdTomato positive cells (sorted at day 5), *Nanog*-GFP and *Mir290*-RGM positive cells (sorted at d10-14), and "double negative" cells (sorted at d5). The cells were seeded as single cell-per-well, and were treated with medium either supplemented with Dox or lacking Dox. On day 14 colonies were inspected for GFP and mCherry (RGM) markers.

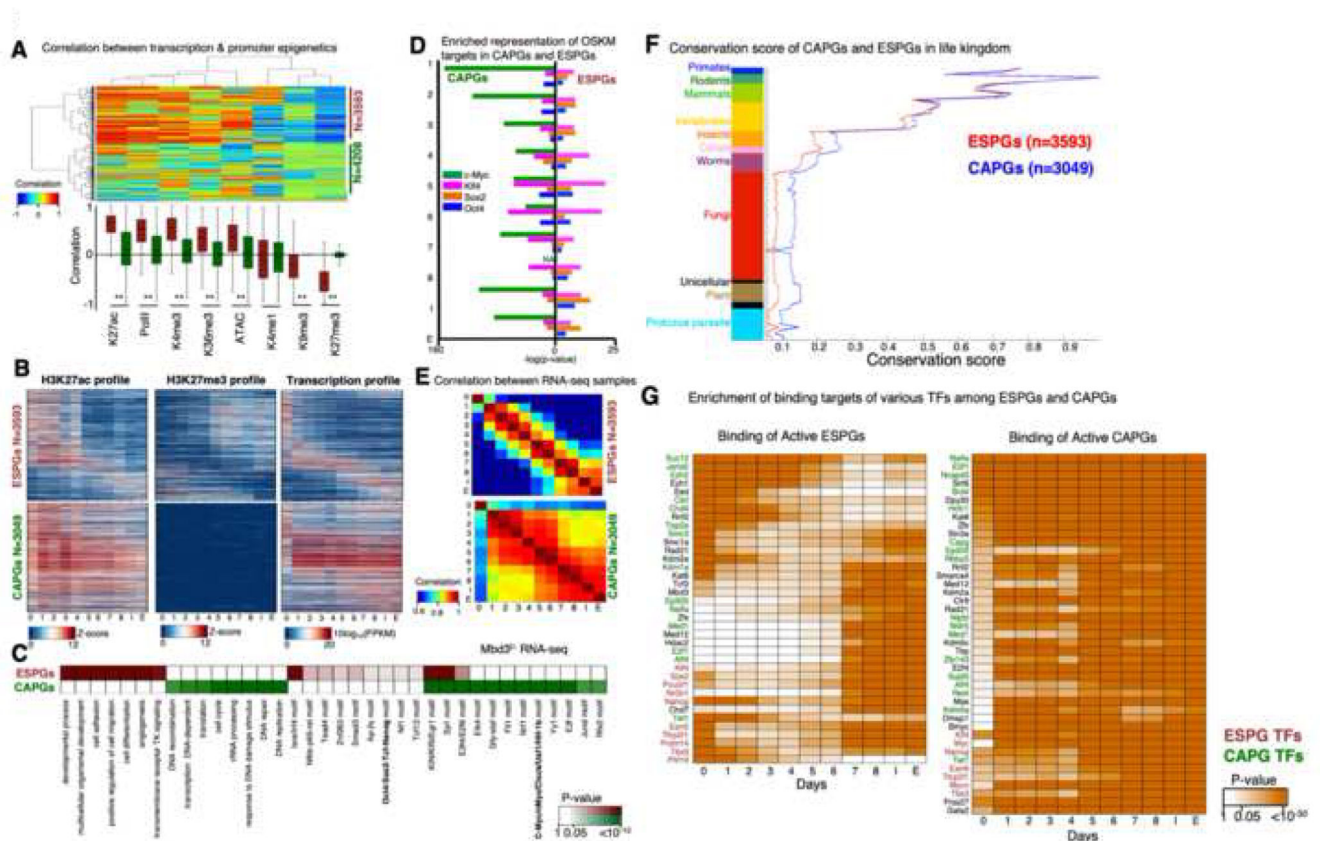


**Fig. 4. Distinct regulation of cell fate genes and of biosynthetic processes by MYC.**

**A.** Spearman correlation between the expression change of each differential gene (row) and change in promoter chromatin modification of each indicated mark (column). Analysis was done on all differential genes that have at least two marks in their promoter (i.e. with z-score > 1 std), resulting in 7801 genes. Hierarchical clustering clustered the genes into two distinct groups: genes with correlation between gene expression and promoter epigenetic modifications (n=3593) and genes with no trend of correlation (n=4208). Top: clustered correlation matrix. Bottom: correlation distribution of each mark in the two gene groups, where red denote correlated group, and green denote the non-correlated group. \*\*Wilcoxon p-value <  $10^{-170}$

**B.** Pattern of H3K27ac, H3K27me3 and expression in Epigenetically Switched Genes (ESPGs, top), and in genes with Consistency-Active-Promoters (CAPGs, bottom). Each row corresponds to a single gene, genes are sorted according to their expression pattern and the same sorting was applied to the epigenetic marks.

**C.** Enrichment of GO categories and binding motifs in ESPGs (red), CAPGs (n=3049, green). Color shades indicate FDR corrected Fisher exact test p-value, or motif enrichment p-value.

**D.** Enrichment of OSKM binding targets in promoters of ESPGs compared to CAPGs. Minus log<sub>10</sub> of Fisher exact test p-values are indicated.

**E.** Spearman correlation matrix between Mbd3<sup>f/-</sup> RNA-seq samples calculated over ESPGs (Top), showing a gradual change along reprogramming and over CAPGs (Bottom), showing two waves of change, on day 1, and on days 5-6.

**F.** Conservation score of ESPGs and CAPGs calculated with Phylogene software<sup>74</sup>. Graph includes the mean and SEM values for each gene set (one tailed Wilcoxon

test, p-value of nonvertebrate organisms  $<10^{-30}$ ). **G.** Scheme showing transcription factors that significantly bind ESPGs or CAPGs that are active in each day of reprogramming, based on ChIP-seq databases. Red – ESPGs transcription factors, Green – CAPGs factors. Orange shades – FDR corrected p-values (Fisher exact test).

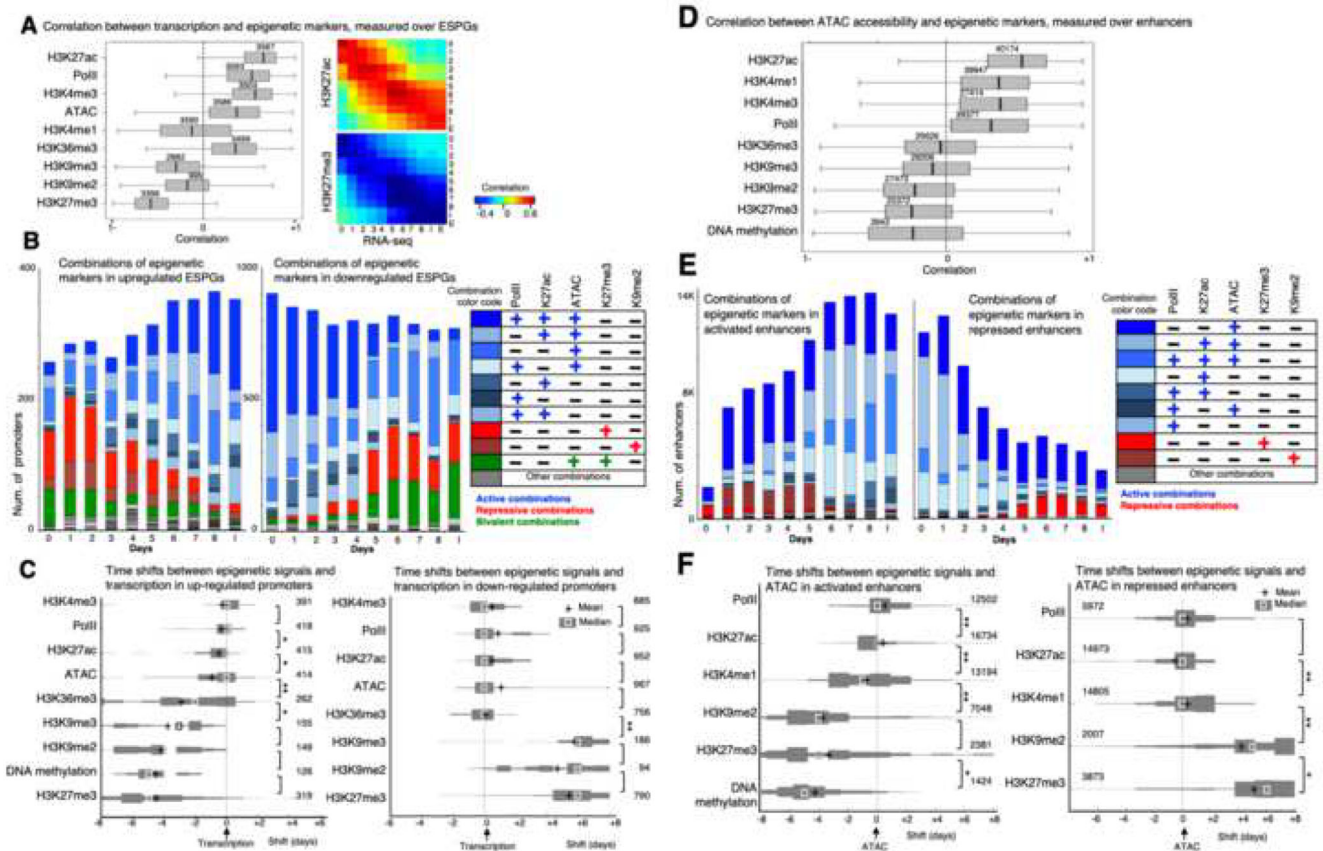


**Fig. 5. Mapping the order of epigenetic events that drive transcription initiation and repression**

**A.** Left: Correlation between each of the indicated chromatin modifications and gene expression patterns that were measured in the promoters of ESPGs that have the modifications (numbers are indicated). Correlations were calculated for each gene, over 11 time points. H3K27ac, PolII and H3K4me3 show positive correlation with gene expression, while H3K27me3 and to lesser extent H3K9me2,3 show negative correlation with expression. Right: Correlation matrix over all ESPGs, between H3K27ac or H3K27me3 and gene expression (RPKM) for each sample separately. **B.** Stacked bar chart of all combinations of the indicated chromatin modifications, as measured in promoters of upregulated ESPGs (left) and downregulated ESPGs (right). Right – color code of frequent combinations (>3% of each sample). **C.** Distribution of time shifts between each of the indicated epigenetic modification and gene expression profile, measured using cross correlation. The distribution, presented as histogram, was measured over upregulated ESPGs (Left) and downregulated ESPGs (right) which have a changing epigenetic modification (max-min z-score > 0.5). The number of promoters tested is indicated. X-axis indicates the temporal time shift in days. Plus indicates mean, and square indicates median. \* $p < 10^{-5}$ , \*\* $p < 10^{-25}$  (Wilcoxon test). **D.** Correlation between each of the indicated chromatin modification and DNA accessibility patterns that were measured in all differential enhancers that have the modifications (numbers are indicated). Correlations were calculated over 11 time points. **E.** Stacked bar chart of all combinations of the indicated chromatin modifications, as measured in activated enhancers (left) and in repressed enhancers (right).



Right – color code of frequent combinations (>3% of each sample). **F.** Distribution of time shifts between each of the indicated epigenetic modification and accessibility profile, measured using cross correlation. The distribution, presented as histogram, was measured over activated enhancers (Left) and repressed enhancers (right) which have a changing epigenetic modification (max-min z-score > 0.5). The number of enhancers tested is indicated. X-axis indicates the temporal time shift in days. Plus indicates mean, and square indicates median. \*  $p < 10^{-4}$ , \*\*  $p < 10^{-50}$  (Wilcoxon test).

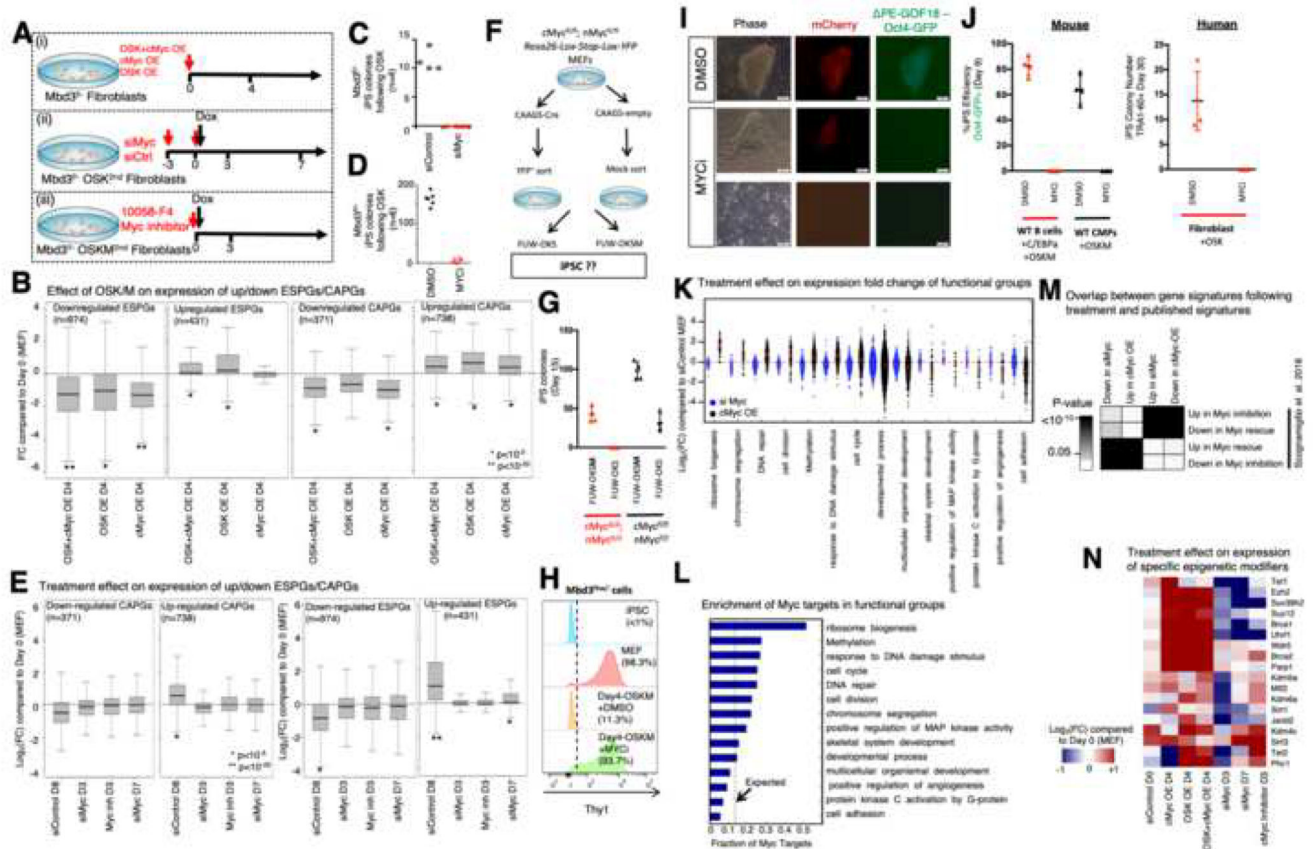


**Fig. 6. Biosynthetic processes are regulated by Myc activity.**

**A.** Experimental flow describing three experimental perturbation settings: (i)  $Mbd3^{fl/fl}$  MEFs were virally infected with cMyc over-expression (OE) cassette, OSK-OE cassette or both cassettes. Gene expression was measured on day4 following infection. (ii)  $Mbd3^{fl/fl}$  MEFs carrying OSK Dox-dependent cassette were treated for knockdown of c-Myc, n-Myc and l-Myc. Gene expression was measured on days 3 and 7, and colony formation was measured on day 11. (iii)  $Mbd3^{fl/fl}$  MEFs carrying OSKM Dox-dependent cassette were treated with inhibitor of cMyc (10058-F4) and with Dox. Gene expression and colony formation were measured on day 3. **B.** Distribution of Expression fold change (FC) compared to WT MEF of up/down regulated ESPGs (down regulated ESPGs are enriched for somatic genes), and CAPGs. Presented perturbations are over-expression of OSK cassette, over-expression of c-Myc cassette, or over-expression of the two cassettes together. (\* $p < 10^{-5}$ , \*\* $p < 10^{-20}$ , Wilcoxon test). **C-D.** Reprogrammed colony formation in Myc knockdown or small molecule inhibition, measured 11-14 days after Dox. **E.** Distribution of expression fold change (FC, in log2 scale) compared to MEF of up/down regulated ESPGs and CAPGs. Presented perturbations are Myc knockdown, inhibition of Myc activity with small molecular inhibitor (10058-F4). (\* $p < 10^{-5}$ , \*\* $p < 10^{-20}$ , Wilcoxon test). **F.** Experimental scheme. **G.** IPSC Reprogramming efficiency in different cells expressing both endogenous and/or exogenous cMyc and nMyc. **H.** FACS analysis for surface expression of fibroblast surface marker Thy1 on the indicated  $Mbd3^{fl/fl}$  cell types. Dotted line indicates positive threshold for detection. **I.** Representative pictures of  $Mbd3^{fl/fl}$  cells harboring mCherry-NLS



and PE-GOF18 Oct4-GFP cassettes after 13 days of reprogramming in the presence of MYCi. Scale = 100 $\mu$ M. **J.** Left panel - iPSC reprogramming efficiency by applying highly efficient mouse B cell and WT CMP reprogramming protocols by OSKM in the presence or absence of MYC small molecule inhibitor (MYCi). Right panel – Human iPSC reprogramming efficiency by applying OKS lentiviral transduction in the presence or absence of MYCi. **K.** Expression fold-change distribution (log<sub>2</sub> scale) of selected GO categories in Myc over-expression or Myc knockdown, showing that upon over-expression of Myc, processes such as ribosomal biogenesis and chromosome segregation are induced. **L.** Fraction of Myc targets in significantly induced and repressed GO categories, compared to what is expected by random (dashed line). **M.** Overlap between differential genes detected in Myc perturbation experiments, and differential genes detected in previous published perturbations (Scognamiglio et al., 2016). Fisher exact test p-values are presented. **N.** Expression fold change of selected chromatin modifiers.

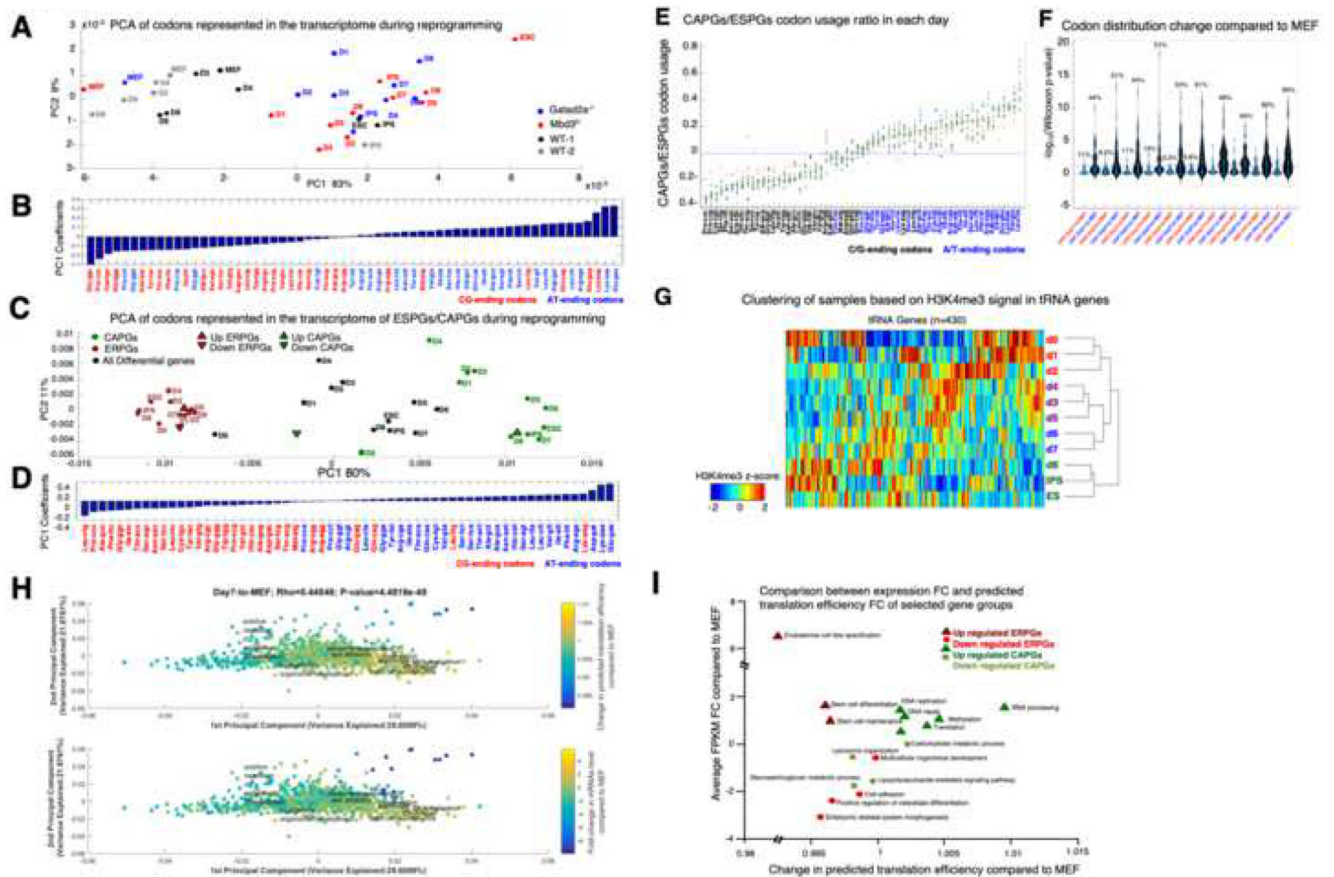


**Fig. 7. Biosynthetic processes are coordinated by optimization of available tRNA pool.**

**A.** A PCA projection of codons' representation in the transcriptome along reprogramming in  $Mbd3^{fl}$ ,  $Gata2a^{-/-}$  and the two WT systems. The representation of the codons in the transcriptome was determined by multiplying the number of occurrences of each codon in each gene by the scaled expression level of each gene in each time point/cell type. The variance percentage, out of the total original variance in the high-dimensional space, spanned by the first and second PCs is indicated on the x and y axis, respectively. **B.** Coefficients associated with first principle component of **A**. **Blue** – A/T ending codons, **Red** – G/C ending codons. **C.** A PCA projection of the codon usage of all differential genes (black), ESPGs (red) and CAPGs (green) show a striking separation between ESPGs and CAPGs. **D.** Coefficients associated with first principle component of **C**. **E.** Distinct and rapid change in codon usage is specific to CAPGs. ESPGs prefer G/C-ending codons, while CAPGs use A/T-ending ones. Scatter plot analysis of the CAPGs-to-ESPGs ratio of codon usage. For each codon, shown are 11 calculated CAPGs-to-ESPGs ratios of codon usage along reprogramming and in ESCs. The mean and median values of each codon are shown as red crosses and green squares, respectively. Three time points are color-coded: red = CAPGs-to-ESPGs ratio in MEF; blue = CAPGs-to-ESPGs ratio in iPS; light blue = CAPGs-to-ESPGs ratio in ES. **F.** CAPGs change significantly their codon usage compared to MEF already in day 1 of reprogramming, where ESPGs are much less variable. Violin plot of the significance ( $-\log_{10}(\text{Wilcoxon p-value})$ ) of the differences between the usage of each of the

61 sense codons in each day compared to MEF, calculated for ESPGs (red) and CAPGs (blue) sets (for each day separately). **G.** Hierarchical Clustering of various time points/cell types based on the H3K4me3 signature in the vicinity of individual tRNA genes. (n=430, Spearman correlation metric and average linkage were used). **H.** Projection of the tRNA translation efficiency and mRNA expression changes on the Codon-Usage Map. PCA projection of GO category gene-sets. The location of each gene set in this space is determined by the average codon usage of all the genes that belong to it. The % variance spanned by the first and second PCs is indicated on the x and y axis, respectively. The color code represents the predicted translation efficiency of tRNAs and expression change of mRNAs (upper and lower panels, respectively) in day1 compared to MEF. **Top:** each gene category is color coded according to the relative change in the availability of the tRNAs that correspond to the codon usage of its constituent genes, averaged over all genes in the category; the tRNA availability of each individual gene was calculated similarly to the tAI measure of translation efficiency, where the expression of individual tRNA genes was evaluated by the H3K4me3 reads in its vicinity. A red color for a given gene category indicates that on average the genes in that category have codons that mainly correspond to the tRNAs that are induced in day1, whereas a blue color indicates that the codon usage in the categories is biased toward the tRNAs that were repressed in day1. **Bottom:** Changes at the mRNA level, averaged over all the genes in each gene category as in the upper panel, where here too red means that the genes were induced in day1. **I.** Comparison between predicted changes in translation and changes in transcription for various GO categories that show the highest association with up/downregulated CAPGs/ESPGs.